

Chapter 10

Iron-Based Intermetallics



Martin Palm and Frank Stein

Abbreviations and Symbols

a_0	Lattice constant a
A2	Strukturbericht symbol
AIM	Air induction melting
at.%	Atom percent
B2	Strukturbericht symbol
B20	Strukturbericht symbol
BDTT	Brittle-to-ductile transition temperature
b.c.c.	Body-centered cubic
$^{\circ}\text{C}$	Degrees centigrade
cm	Centimeter
cP8	Pearson symbol
CVD	Chemical vapor deposition
D8 ₈	Strukturbericht symbol
D0 ₃	Strukturbericht symbol
$\dot{\epsilon}$	Strain rate
E_{Corr}	corrosion potential
ESR	Electroslag remelting
f.c.c.	Face-centered cubic
g	Gram
GPa	Gigapascal
h	Hour
hcp	Hexagonal close-packed

M. Palm (✉) · F. Stein

Department Structure and Nano-/Micromechanics of Materials, Max-Planck-Institut für Eisenforschung GmbH, Düsseldorf, Nordrhein-Westfalen, Germany

e-mail: palm@mpie.de; stein@mpie.de

hP6	Pearson symbol
hP16	Pearson symbol
HCF	High-cycle fatigue
k_p	Parabolic rate constant
L2 ₁	Strukturbericht symbol
LMD	Laser metal deposition
m	Meter
μB	Bohr magneton
MPa	Megapascal
μm	Micron meter
oC48	Pearson symbol
Ω	Ohm
ORNL	Oak Ridge National Laboratories
s	Second
$\sigma_{0.2}$	0.2% yield stress
SCE	Saturated calomel electrode
SOFC	Solid oxide fuel cell
T_C	Curie temperature
TCP	Topological close-packed
tP3	Pearson symbol
TRIP	Transformation-induced plasticity
TRW Inc.	Thompson Ramo Wooldridge Incorporated
US	United States
V	Voltage
VIM	Vacuum induction melting
vol.%	Volume percent
wt.%	Weight percent
YSA	Yield stress anomaly

10.1 Introduction

Intermetallic phases – commonly abbreviated as intermetallics – are phases which have different crystallographic structures than the elements they constitute of [1]. They can appear as precipitates, e.g., Laves, μ , or σ phase in steels, or form the base material like FeAl and Fe₃Al in iron aluminide-based alloys or Fe₃Si in Fe–Si alloys. The ordered intermetallic phases are usually rather strong, and many of them are stable up to high temperatures. Therefore, they have been considered as strengthening precipitates since long.

The most prominent example of precipitation hardening of steels by intermetallic phases are classical maraging steels. In these low-carbon steels with Ni contents of about 12–25 wt.% and additions of Ti, Al, Nb, Mo, Co etc., finely distributed intermetallic phases are precipitated when martensite transforms to austenite during aging (maraging) at 400–500 °C [2, 3]. Which intermetallic phases form depends

on alloy composition, temperature, and time of maraging. Besides (Ni,Fe)Al, Ni₃Ti, Ni₃Mo, and NiTi, the σ -phase FeMo and the Laves phases Fe₂Ti and Fe₂Mo are frequently observed intermetallic precipitates. The fine intermetallic precipitates effectively hinder the movement of dislocations. The resulting high-strength steels are, e.g., used as tool steels for application at high temperature. More recently, the concept of maraging has been transferred to other steels and combined with the transformation-induced plasticity (TRIP) effect [4]. On the other hand, Laves and σ -phases have been considered as detrimental in steels and superalloys because they may cause grain boundary embrittlement [5–7] and a loss in creep strength after prolonged service [8].

This chapter focuses on ferrous materials that are based on intermetallics, i.e., iron aluminides and iron silicides, as well as ferrous materials which gain these properties from specific microstructures achieved by intermetallic phases.

10.2 Iron Aluminides

Alloys based on the phases Fe₃Al and FeAl are lightweight (densities 5.7–6.7 g/cm³) Fe-based materials with high wear resistance and excellent corrosion resistance. For applications, alloys in the composition range between about 15 and 40 at.% Al (8–24.5 wt.% Al) are of specific interest. The lower value corresponds to the Al content necessary to form protective Al₂O₃ scales; above the upper value the alloys become inherently brittle. Already around 1900 it was recognized that Fe becomes wear and oxidation resistant by alloying with Al. From the 1940s onward, numerous alloy developments were carried out, however usually with the outcome that brittleness and insufficient strength at high temperatures precluded their industrial application. New alloy concepts and economic pressure to minimize the use of strategic elements have revived industrial interest in these alloys in recent years [9].

10.2.1 Phases and Phase Diagram

Figure 10.1 shows the Fe–Al phase diagram. The liquidus temperatures in the Fe–Al system were established in 1908 and the outline of the phase equilibria by 1930, and then the first compendium on binary phase diagrams already contained a version, which was close to the present one [10]. The system contains six intermetallic phases in all. The three Al-rich phases FeAl₂, Fe₂Al₅, and Fe₄Al₁₃ all have low-symmetrical crystal structures, which make them rather brittle. They have only limited homogeneity ranges and melting temperatures between 1150 and 1158 °C. The phase Fe₅Al₈ is only stable above 1095 °C and decomposes eutectoidally even during quenching.

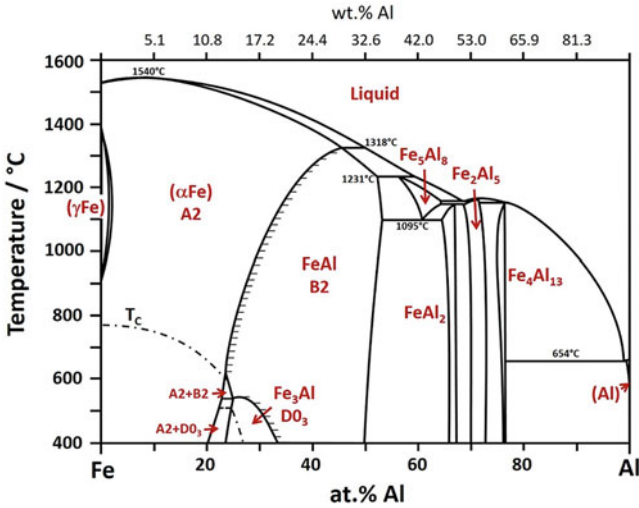


Fig. 10.1 Fe–Al phase diagram constructed on the basis of [11] with changes in the Al-rich part according to [12]

In view of structural applications, the two Fe-rich phases Fe₃Al and FeAl are of interest. The cubic D0₃-ordered phase Fe₃Al is stable between about 23 and 36 at.% Al and up to a temperature of 545 °C. B2-ordered FeAl is also cubic. It has a wide homogeneity range between 23 and 53 at.% Al and is stable up to 1318 °C. On heating, Fe₃Al transforms to FeAl by a second-order transition. Alloys of up to 45 at.% Al transform from FeAl to disordered cubic (αFe), and the transition temperatures increase markedly with increasing Al content. On cooling both transformations cannot be suppressed by quenching.

10.2.2 Alloy Developments

The first reports about “aluminum steels” and Al in cast iron date from 1890 [13, 14]. By the 1930s patented alloys existed in Russia (Cugal) and in Britain [15, 16]. The first better documented alloy developments are Alfenol and Thermenol by the US Naval Ordnance Laboratory and Pyroferal in former Czechoslovakia in the 1950s. Alfenol was originally developed for magnetic applications. The binary alloy contained 28.3 at.% Al (16 wt.%) of which strips and tapes were produced by hot and cold rolling [17]. Thermenol is a Fe–Al–Mo-based alloy designed for high-temperature use, e.g., for jet engine compressor blades [18]. Both alloy developments were continued at the Ford Motor Company in conjunction with the Wright Air Development Center and resulted in the production and testing of a number of parts, e.g., heat treatment boxes and a turbine exhaust cone [19–21].

Other alloy developments at this time in the USA to note are “DB-2” a Fe–Al–Cr–Nb–Zr-based alloy at The Martin Company and Fe–Cr–Al alloys at the Battelle Memorial Institute [22, 23]. Pyroferal is a Fe–Al–C-based alloy, with an Al content of 44.5–46.5 at.%, from which various cast parts for use in industrial furnaces were produced on a larger scale [24, 25]. Thermagal denotes a series of Fe–Al–C-based alloys developed in the 1960s in France and was used to produce a large variety of parts, e.g., crucibles, apparatuses for chemical industries, parts for mineral crushers, heating elements, permanent magnets, etc. [26]. Activities on Alfenol and specifically Thermenol were continued until the early 1970s under contract of the Office for Saline Water in search for corrosion-resistant tubes for seawater desalinization [27]. Pratt & Whitney and TRW Inc. under contract of the Air Force Wright Aeronautical Laboratories investigated the potential of Fe–Al alloys for application in aircraft engines in the 1980s [28, 29].

The alloy developments pursued at Oak Ridge National Laboratories (ORNL) are most prominent. Already involved in the study of dispersion-strengthened iron aluminides in 1960 [30], ORNL started large-scale activities on the development of iron aluminide-based alloys in the mid-1980s within the Fossil Energy Materials Program of the US Department of Energy. Series of alloys termed FA, FAL, FAS, etc. were developed and extensively characterized, and processing was studied in detail involving numerous industries. The work yielded a substantial understanding of iron aluminide alloys and is well documented in the Proceedings of the Annual Conference on Fossil Energy Materials and a number of review papers [31–35].

Other more recent activities to note are the development of the Al-rich oxide dispersion-strengthened alloy Grade 3 in France [36] and Fe–Al–C-based alloys in India at the Defense Metallurgical Research Laboratory [37, 38]. Also at the authors’ institution, research on iron aluminides has a long tradition. Currently, at authors’ institution alloys are developed using a variety of alloying concepts, and their processing and behavior under application conditions is studied in cooperation with industry [39].

10.2.3 Peculiar Features of Iron Aluminides

Iron aluminides show three peculiar features: unusual high vacancy concentrations, a yield stress anomaly (YSA) and environmental embrittlement. As all of them strongly influence the mechanical behavior, understanding these features is essential to assess the mechanical behavior of iron aluminide alloys.

FeAl and Fe₃Al both have low enthalpies for the formation of constitutional vacancies and therefore can contain up to 2 vol.% of vacancies at room temperature [40, 41]. The quenched-in vacancies have a strong hardening effect by lowering the mobility of dislocations, and therefore the yield strength at room temperature for a given alloy can vary by two to five times in dependence on the vacancy concentration [42, 43]. As the amount of quenched-in vacancies increases with increasing cooling rate, processing has a marked influence on the yield strength.

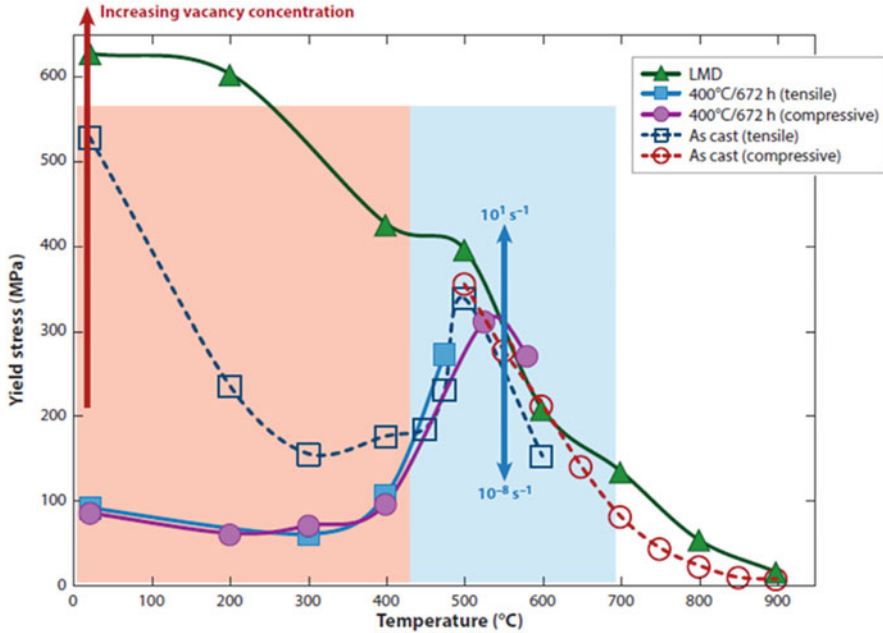


Fig. 10.2 Tensile or compressive $\sigma_{0.2}$ yield stress of binary Fe–Al with 26–28 at.% Al at a strain rate of $\dot{\epsilon} = 1 \times 10^{-4} \text{ s}^{-1}$. In the orange shaded area, the yield strength is dominated by quenched-in vacancies: high vacancy concentration after rapid cooling after laser metal deposition (LMD), intermediate vacancy concentration after moderate cooling during casting, and minimum vacancy concentration after annealing at 400 °C for 672 h. The blue shaded area denotes the temperature range where the yield stress is affected by the yield stress anomaly (YSA), where the blue arrow indicates the dependence of the YSA on deformation rate. (Figure taken from Ref. [9])

A minimum of quenched-in vacancies can be attained by annealing at 400 °C for 100 h [44]. Figure 10.2 shows the influence of varying vacancy concentrations on the $\sigma_{0.2}$ yield stress of binary Fe–Al.

Between about 400 °C and 600 °C, iron aluminide-based alloys show an increase of the yield strength with increasing temperature, a feature not unusual for ordered intermetallic phases (Fig. 10.2). As the yield strength is expected to decrease with increasing temperature, this phenomenon has been termed yield stress anomaly (YSA). In the case of the iron aluminides, the YSA is caused by a change in the dislocation structure at these temperatures, decomposition of superdislocations creating local pinning points, and interaction of the debris with quenched-in vacancies [45–50]. The YSA is strongly strain rate dependent, decreasing with decreasing strain rate and vanishing at strain rates below $1 \times 10^{-7} \text{ s}^{-1}$ [51, 52] (Fig. 10.2). The practical implications are that the YSA makes hot forming between 400 and 600 °C difficult while it does not contribute to strengthening during creep. It is also noted that the actual yield strength at the maximum of the YSA and the temperature where this maximum occurs can be markedly influenced by alloying.

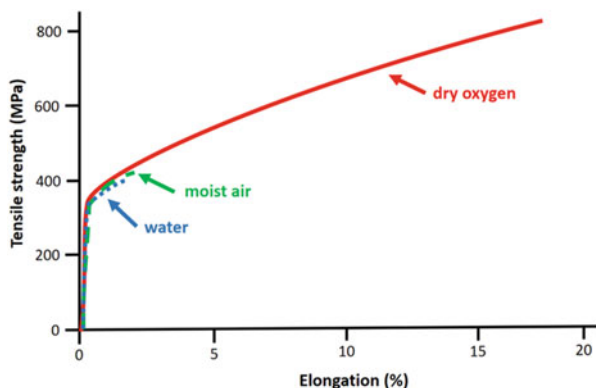


Fig. 10.3 Tensile yield stress of binary Fe–Al in different test environments. (Reproduction of the classic experiments by C.T. Liu et al. as shown in Ref. [31])

Fe₃Al- and FeAl-based alloys usually show a limited ductility of 2–4% total elongation at room temperature, which is still not bad compared to other intermetallic phases. Both phases are ductile when tested in hydrogen-free environments but fail in a brittle manner in the presence of moisture or hydrogen (Fig. 10.3). This phenomenon is termed environmental embrittlement and is caused by an embrittlement of crack tips by hydrogen, which is produced by the reaction $3\text{H}_2\text{O} + 2\text{Al}^{3+} \leftrightarrow 6\text{H}^+ + \text{Al}_2\text{O}_3$ [53, 54]. A detailed review on the topic is given by Zamanzade and Barnoush [55].

10.2.4 Strength, Ductility, Fatigue, Wear, and Erosion

Lack in strength at high temperatures has been the main obstacle for a wider use of iron aluminides. Therefore a substantial part of the research on iron aluminides has been devoted to evaluate different strengthening mechanisms [56–61].

Binary Fe–Al alloys lose their strength when Fe₃Al transforms to FeAl, i.e., at 545 °C at the latest. Solid solution hardening by a third element is well possible as many elements have a large solid solubility in Fe₃Al and FeAl. By solid solution hardening, the yield strength can be markedly raised, e.g., by alloying with 4 at.% V, Ti, or Mo, the yield strength can be increased from about 20 MPa to about 95–115 MPa at 800 °C [61] (Fig. 10.4).

In analogy to steels, much work has been devoted to strengthen iron aluminide-based alloys by carbide precipitates. However, no substantial strengthening has been achieved. For Fe–Al–C alloys containing Fe₃AlC precipitates, the yield strength drops markedly above 600 °C and equals that of a precipitate-free alloy of same Al content at 800 °C [64, 65] (Fig. 10.4). Fe–Al–X–C alloys with different carbide precipitates and additional solid solution hardening of the matrix show a less

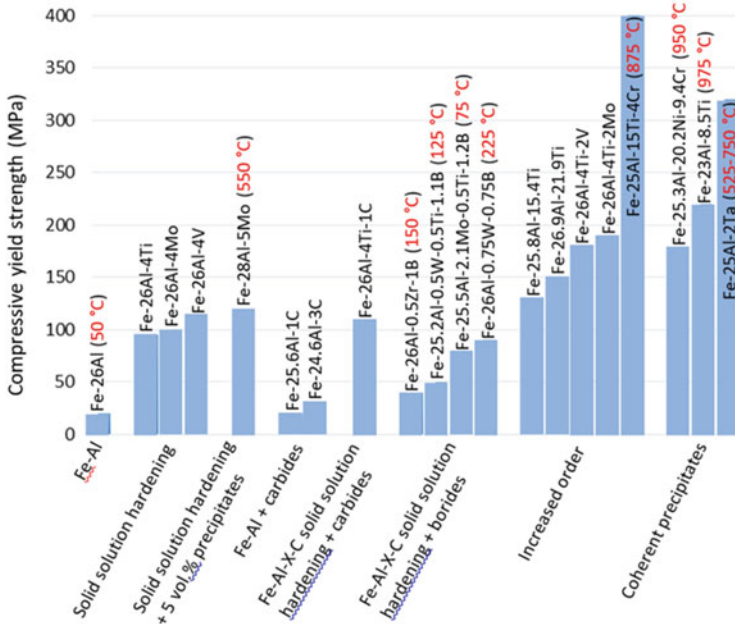


Fig. 10.4 Compressive yield strength at 800 °C of iron aluminide alloys containing 23–28 at.% Al and strengthened by different mechanisms (strain rate $\dot{\epsilon} = 1 \times 10^{-4} \text{ s}^{-1}$). Temperatures given in red indicate brittle-to-ductile transition temperatures. (Data from Refs. [61–74])

pronounced decrease of the yield strength above 600 °C, but with about 110 MPa, they only show about the same strength as solid solution hardened alloys [65] (Fig. 10.4). Analysis of published data shows that carbides have a limited strengthening effect above 600 °C and no effect at 800 °C. Reasons are difficulties to attain an even distribution of fine carbide precipitates, which effectively hinder dislocation movement and rapid coarsening of carbides at high temperatures.

Borides have about the same limited strengthening effect as carbides, but they may form finer precipitates, which do not coarsen at high temperatures [75] (Fig. 10.4). Precipitation hardening by another intermetallic phase is also possible, specifically by Laves phases, as in many Fe–Al–X systems, respective phase equilibria between Fe₃Al or FeAl and a Laves phase exist [61]. As Laves phases have a much higher strength than the iron aluminides, strengthening will depend on the volume fraction of the precipitates. Though this would yield in principle very strong alloys, again generation of fine and evenly distributed precipitates is very difficult, and respective alloys are therefore rather brittle [76]. However, in a few Fe–Al–X systems, the precipitated Laves phase forms a film on the iron aluminide grain boundaries, and such alloys show an appreciable strength [77]; see Sect. 10.5. For strengthening by the formation of coherent microstructures involving α -Fe, FeAl, and Fe₃Al/Fe₂XAl, see Sect. 10.4.

Iron aluminides lose their strength when f.c.c. Fe_3Al transforms to b.c.c. FeAl ; therefore stabilizing the f.c.c. structure at higher temperatures by alloying is another viable method to increase their strength. Actually the transition temperature can be raised substantially by a number of elements, most prominently by Ti up to 1212 °C [78]. Respective alloys can have a yield strength of about 400 MPa at 800 °C but are also rather brittle [68] (Fig. 10.4).

With respect to creep resistance, the various strengthening concepts are as effective as for increasing the yield strength. Compared to the advanced Cr-containing steel P92, iron aluminide-based alloys containing carbide or boride precipitates show an inferior creep resistance at 650 °C, while those strengthened by coherent precipitates or those with Fe_2XAl matrix can have substantially higher creep resistance [39].

As for other materials, strengthening of iron aluminide-based materials in most cases reduces the limited ductility even more [79]. While the change from brittle to ductile behavior for binary Fe_3Al and FeAl gradually takes place until about 100 °C where the alloys are ductile, ternary and higher-order alloys usually show a marked brittle-to-ductile transition temperature (BDTT), which can be higher than 800 °C [39] (Fig. 10.4). Until today, no general principle for increasing the ductility of iron aluminide-based materials has been found. Reduction of the grain size below about 10 μm , optimizing the Al content, and alloying with boron for a better cohesion of the grain boundaries and with chromium to reduce the effect of environmental embrittlement have been suggested for maintaining or even improving ductility [31, 60, 80, 81]. However, none of these methods is without exemption, and their effects are limited.

As iron aluminides show rather quick coarsening at elevated temperatures, control of the grain size, e.g., by precipitates at the grain boundaries, is important. It has also been shown that thermomechanical processing can increase the ductility compared to their as-cast counterparts. Minimizing the amount of quenched-in vacancies may also enhance ductility. Still ductility may be limited to 2–4%, but this has proven to be sufficient for many applications.

Comparable few data are available for fatigue of iron aluminides, and as these data have been obtained on a variety of alloys and by different tests, general trends are difficult to identify [82]. Studies of the fatigue crack growth in Fe_3Al - and FeAl -based alloys revealed that environmental embrittlement by moist air again has a major effect, though no straightforward relation between ductility under static loading and cyclic loading has been found [83, 84]. Other observations were that alloys with coherent (αFe) + Fe_3Al microstructures showed a higher resistance against high-cycle fatigue (HCF) than single-phase Fe_3Al , and it was found that the anomalous strengthening in the temperature range of the YSA does not necessarily result in an increased fatigue life [85, 86].

Iron aluminides possess a good to excellent wear resistance, and, therefore, quite a number of investigations have been performed [87, 88]. In view of the variety of test methods, test conditions, and tested alloys, it is again difficult to find general trends.

Because of their good wear resistance, iron aluminides have not only been explored as bulk alloys but also as coatings, as binder for cemented hard phases, or as hard phase in a ductile binder. Wear resistance increases with increasing hardness, which increases with the Al content in binary Fe–Al alloys, by the formation of an Al_2O_3 oxide scale, through alloying, or by addition of a hard second phase. The beneficial effect of an oxide scale in improving wear by reducing scuffing has been attributed to its higher hardness and the ceramic nature of the scale [89]. Environmental embrittlement again may have some influence, because a decrease in wear resistance has been observed during wet abrasion [90].

The erosion behavior of iron aluminide alloys and cermets shows a ductile behavior [91]. The erosion resistance increases with increasing Al content, which is explained by an increase of strain hardening rates, leading to rapid work hardening of the surface, which limits deformation to a shallow region [91]. Specifically at high temperatures in oxidizing atmospheres, the erosion behavior of an iron aluminide can be favorable compared to steel [88].

10.2.5 Corrosion

The outstanding corrosion resistance of Fe_3Al and FeAl is related to their ability to readily form passive layers or thin and adherent oxides scales, for which, depending on environmental conditions, a minimum of 15–18 at.% Al is necessary (Fig. 10.5). Specifically in oxidizing atmospheres, they form Al_2O_3 scales which have parabolic rate constants up to two magnitudes lower than for Cr_2O_3 -forming alloys, and, therefore, Fe_3Al and FeAl show a better oxidation resistance in many environments [56, 92–94]. Al_2O_3 scales are also protective in many other corrosive environments. For example, resistance against metal dusting, i.e., disintegration of Fe-based materials due to carburization, can be markedly improved [95, 96]. For protection in nonoxidizing environments, the scale can be generated by pre-oxidation.

The aqueous corrosion resistance of iron aluminides is considered not to be good [97]. Electrochemical studies of the aqueous corrosion resistance of Fe–Al have already been reviewed some time ago [98]. Fe_3Al and FeAl passivate by forming films consisting of Al- and Fe-hydroxides or oxides. The aqueous corrosion behavior of Fe–Al depends on the electrolyte. While they show passivation in neutral and alkaline electrolytes, corrosion rates are moderate to high in strong acids, specifically in the presence of Cl^- . Passivation can be improved by alloying with Cr and/or Mo [99]. Recently it has been shown that the aqueous corrosion resistance can be markedly improved through generating an Al_2O_3 scale by pre-oxidation [100]. Immersion tests in seawater and neutral salt spray tests showed that the corrosion resistance improved with increasing Al content and that dense layers of Fe_3O_4 (magnetite) form under these conditions [27, 101].

Corrosion by salt deposits or salt melts at high temperatures (hot corrosion) has been investigated as well [35]. Also under these conditions, iron aluminides show

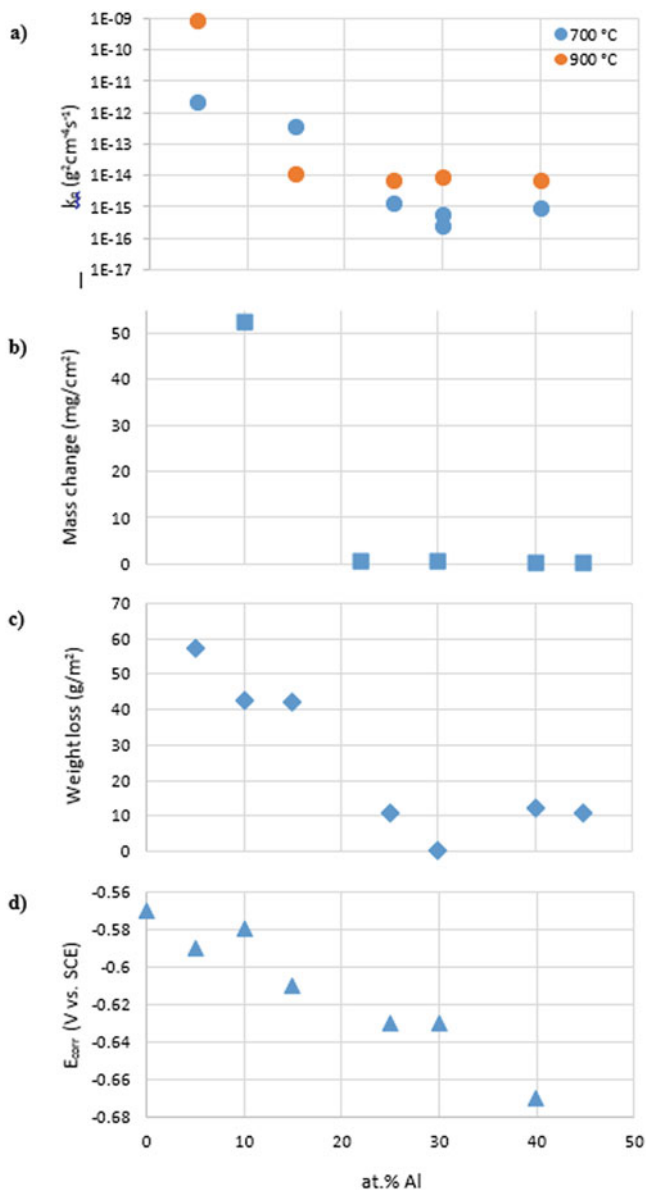


Fig. 10.5 Corrosion resistance of binary Fe–Al in dependence on Al content; (a) parabolic rate constants k_p for oxidation in synthetic air at 700 °C and 900 °C [104]; (b) mass change after exposure in steam at 700 °C for 672 h [105]; (c) weight loss after neutral salt spray testing for 168 h [101]; (d) corrosion potential in deaerated 0.0126 M H_2SO_4 at 25 °C [100]

an excellent corrosion resistance if oxidation is the prevailing corrosion mechanism [102, 103].

10.2.6 *Synthesis and Processing*

Alloys based on the phases Fe_3Al and FeAl can be processed with equipment readily available in steel industry, and process parameters may be similar to those for Cr steels [31, 39, 106]. However, conditions will depend on individual alloys, and thermomechanical processing of alloys with Al contents above about 30 at.% is difficult [107].

Air induction melting (AIM), electroslag remelting (ESR), and the Exo-Melt™ process have been employed for the production of iron aluminide-based alloys on an industrial scale, while a variety of techniques including vacuum induction melting (VIM), arc melting, directional solidification, etc. are used on laboratory scale [31, 108, 109]. Besides producing the alloys from the elements or pre-alloys, production from scrap has also been widely investigated [110–113]. Iron aluminide-based alloys have also been synthesized by various powder metallurgical methods. The strong exothermic reaction between Fe and Al or Al_2O_3 also makes preparation by self-propagating synthesis of alloys and oxide dispersion-strengthened materials feasible [114–116].

Iron aluminides are very well suited for casting as they show good form filling, low porosity, and smooth surfaces, and parts have been produced on an industrial scale by sand casting, centrifugal casting, and investment casting, while strip casting has been employed for rolled products [25, 109, 117, 118] (Fig. 10.6). Careful drying of molds is important to avoid hydrogen porosity, and, as iron aluminide-based alloys tend to form coarse-grained microstructures which may easily crack, respective measures by alloying and/or during casting have to be taken.

Cast or powder metallurgically produced precursors are used for forging, which can be performed in air. Forging of iron aluminides is frequently employed for refining the microstructure, but also parts have been produced on an industrial scale [28, 119–121].

Plates, sheets, and tapes have been produced by conventional hot and cold rolling of iron aluminides with Al contents up to about 30 at.% [107, 122, 123]. At higher Al contents, additional measures have to be taken such as using spacers, canning of the alloys, or use of powder metallurgical precursors, as otherwise severe cracking may occur [124–126]. Rolled products often show increased ductility, and various parts have been produced [122, 127].

As for other intermetallic materials, powder metallurgical processing has been studied intensively. Consolidation of pre-alloyed powders by hot extrusion, often with additions of oxides or borides for increasing strength, has been frequently performed, and steel tubes with an iron aluminum cladding have been produced by co-extrusion of both materials [29, 128–130].

Fig. 10.6 Sand casting of Fe–Al. The melt was produced by AIM, and the part has a diameter of about 600 mm and weighs about 160 kg. (Photograph courtesy of Otto Junker GmbH, Simmerath, Germany)



In order to avoid costly machining, near net shape production by additive manufacturing is currently widely studied. Samples and parts have been successfully produced by all currently available techniques, and additive manufacturing has also been employed for the production of chemically graded materials, e.g., iron aluminide/steel composites [131–134].

Though there have been numerous investigations on processing-property relationships, no final conclusion can be drawn. Regarding strength, quenched-in vacancies have a major influence as detailed above. Therefore, variations in cooling rate after processing at higher temperatures may have a larger effect on strength than variations in processing parameters or even use of different processing routes. For ductility there is some agreement that it should increase with decreasing grain size. However, converse observations have been reported [135]. Any type of further processing usually increases ductility, i.e., decreases BDTT, of as-cast iron aluminide alloys, though the mechanisms are not always clear [136, 137].

Because of their excellent corrosion and wear resistance, iron aluminide coatings have been widely studied, and these activities have been recently reviewed [138, 139]. Machining of iron aluminide-based alloys by all standard techniques has been demonstrated. But as they may show strong work hardening, use of specific tools, shortened tool lifetime, and slower machining speeds may be expected, though not

necessarily so. Nevertheless, economical machining of iron aluminides is a critical issue [140, 141]. Welding of iron aluminides and making iron aluminide/steel bonds has also been evaluated. Cracking due to thermal stresses or by residual hydrogen is an issue and has to be taken care of [142–144].

10.2.7 Applications

Though iron aluminide-based alloys have a great potential and though there have been quite some efforts to make use of this potential for various applications, little has been achieved up to now. Because of their excellent corrosion resistance, iron aluminide-based alloys have been successfully employed as hardware within various industrial furnaces, e.g., for pyrite roasting, carburizing, and glass melting, or in the aluminum industry [21, 25, 109, 117, 145]. Parts for turbines or turbochargers, i.e., where additional benefit is gained from the lower density, are also applications that have been looked at intensively [24, 121, 146]. Other parts for automotive applications that have been produced are exhaust valves and brake discs though published evidence is not in favor of the latter [33, 147]. Different parts for application in marine engines have been tested recently as well [148]. Regarding corrosion- and wear-resistant coatings based on iron aluminides, numerous patents exist, and sintered iron aluminide filter elements for hot gas cleaning are commercially available [149, 150].

10.3 Iron Silicides

Iron alloyed with silicon is a material of tremendous industrial importance since more than 100 years. This is especially because of the excellent soft magnetic properties of electrical steels, which are Fe–Si alloys with silicon contents up to 6.5 wt.% (corresponding to 12.1 at% Si) applied in electric motors, transformers, generators, and static induction devices. However, there are more applications of Fe–Si alloys, for example, making use of the excellent corrosion resistance of Fe_3Si in even very aggressive environments or taking advantage of the magnetic behavior of this intermetallic phase for possible applications in spintronic devices. Below these diverse applications are briefly introduced after a discussion of the binary phase diagram and some remarks on the properties and processing of this type of material.

It should also be mentioned that, as silicon and iron belong to the most frequent elements on earth, iron silicon alloys play a role not only in engineering applications but also in the geological science of the earth core and in the chemistry of terrestrial and extraterrestrial minerals. These aspects will also be briefly described in the following section dealing with the phases and phase diagram of the binary system.

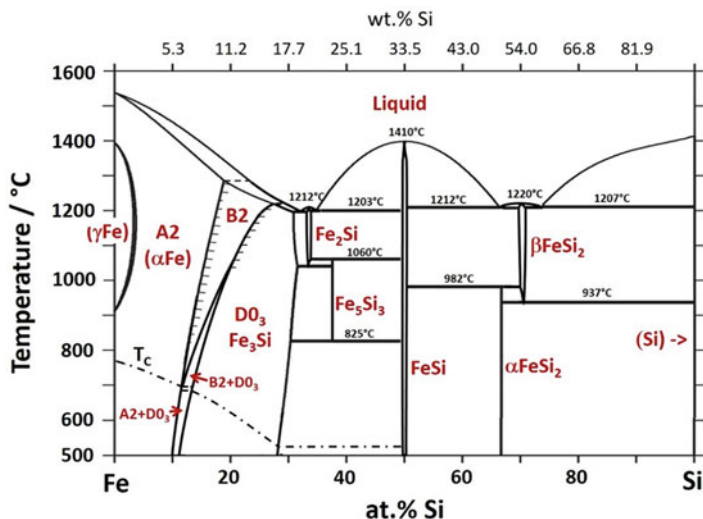


Fig. 10.7 Fe–Si phase diagram constructed on the basis of [151] with changes in the Fe-rich part according to [153]

10.3.1 Phases and Phase Diagram

There is general agreement in the literature about the number and type of intermetallic phases in the Fe–Si system, and the phase diagram version presented in Kubaschewski's classical compilation of Fe binary systems from 1982 [151] remained unchanged for many years and is identical to the phase diagram shown in 2010 in Okamoto's handbook on binary phase diagrams [152]. Only more recently, Ohnuma et al. [153] performed a detailed reinvestigation of the Fe-rich part of the system combining experimental work and thermodynamic calculations, and Cui and Jung included all these data into their thermodynamic reassessment of the system [154]. The phase diagram shown in Fig. 10.7 follows these studies especially including the new results of Ohnuma et al. for the Fe-rich part.

Similar to the Fe–Al system, large amounts of Si can be dissolved in the ferritic α -Fe solid solution, and the ordered B2 and D0₃ (Fe₃Si) superstructures of the A2 b.c.c. lattice can form depending on Si content and temperature. Compared to the Fe–Al system, there is a stronger tendency to ordering occurring already for Si contents as low as 10 at.% (corresponding to about 5 wt.%). Early work by Schlatter, Inden, and Pitsch [155–158] indicated a second-order transition from disordered A2 to ordered B2 with increasing Si content and proved the existence of a two-phase B2 + D0₃ phase field. Later, results from neutron diffraction experiments led to some doubt about the occurrence of B2 at temperatures below 700 °C [159]. This was also discussed in a more recent review on the ordering phenomena in Fe–Si alloys [160]. Following the conclusions of Ohnuma's experimental and theoretical

work [153], the phase diagram in Fig. 10.7 does not contain a B2 phase region below 700 °C, but shows the sequence A2 to A2 + D0₃ to D0₃ with increasing Si content.

The D0₃ ordered Fe₃Si phase exists over a wide composition range up to approximately 30 at.% Si. For Si contents below about 28 at.%, Fe₃Si transforms from D0₃ to B2 ordered structure with increasing temperature. The transformation temperature increases with increasing Si content. On further heating, Fe₃Si alloys with less than about 19 at.% Si undergo an additional transformation from B2 to disordered A2 before melting.

At higher Si concentrations, four more intermetallic phases exist in the Fe–Si system, all of them having only very small homogeneity ranges. Fe₂Si is a high-temperature phase melting congruently at 1212 °C and crystallizing with a hexagonal structure (Pearson symbol hP6) [161]. Another high-temperature phase is Fe₅Si₃, which forms on heating in a eutectoid reaction and decomposes in a peritectoid solid-state reaction. Its crystal structure is of the hexagonal D8₈ type (hP16) [162]. FeSi melts congruently and exhibits a cubic B20-type structure (cP8) [163], while FeSi₂ occurs with two structural variants (low-temperature α -FeSi₂ with an orthorhombic (oC48) and high-temperature β -FeSi₂ with tetragonal (tP3) structure) [164]. The low-temperature phase α -FeSi₂ no longer has a metallic character but shows semiconducting behavior, which is why today it is intensively discussed as an eco-friendly and cheap thermoelectric material [165]. The final phase in the binary system is the Si solid solution, which has an extremely low solubility for Fe, reported to be as low as 3×10^{-5} at.% Fe at 1200 °C [166].

Fe silicides were also found as mineral phases of extraterrestrial origin at various places on the earth [167]. Fe₃Si occurs with its D0₃ ordered structure (gupeite [168]) as well as in a disordered b.c.c. state (suessite [169, 170]), but also the other intermetallic phases Fe₂Si (hapkeite) [171], Fe₅Si₃ (xifengite) [168], FeSi (naquite) [172], and FeSi₂ (linzhiite) [173] were detected in meteorites.

High pressures in the range of several 10–100 GPa strongly affect the phase relations in the Fe-rich part of the Fe–Si system. Neither the disordered ferritic solid solution nor any of the intermetallic phases Fe₃Si, Fe₂Si, Fe₅Si₃, and FeSi are stable under very high pressure. Instead, an Fe-16.4 at.% Si (9 wt.% Si) alloy transforms to a close-packed hexagonal (hcp) structure (similar as does pure Fe). An alloy with 27.5 at.% Si (16 wt.% Si) was found to become two-phase hcp + B2, and Fe-50 at.% Si (33.5 wt.%) adopts a single-phase B2 structure [174, 175]. This is of high importance for the geoscience of the interior of the earth as geochemical models based on cosmochemical arguments suggest that the core of the earth mainly consist of iron and could contain up to 33 at.% Si (20 wt.% Si). Exact composition, temperature, and pressure of the core of the earth are still under discussion [176–178], but an Fe–Si alloy in the inner core most likely is a mixture of hcp and B2 phases as is stated in [174].

10.3.2 Properties

Density and lattice parameter of the disordered Fe solid solution decrease approximately linearly with addition of silicon; the room temperature density decreases from 7.87 g/cm³ for pure Fe to about 7.55 g/cm³ for 10 at.% Si [179–181]. The occurrence of ordering results in a slight shrinkage of the lattice corresponding to a small but clearly measurable increase of the density. As for example, an 1100 °C annealed and slowly cooled alloy with 12.1 at.% Si (6.5 wt.%) has an about 0.15% higher room-temperature density than the same alloy after water-quenching from 750 °C [181].

The vacancy concentration in thermal equilibrium in Fe₃Si reaches high values; an extrapolation to the melting temperature yields a vacancy concentration of 4 vol.% for stoichiometric Fe₃Si [182]. The vacancies are located mainly on the Fe sublattice, and their concentration strongly decreases when deviating from the stoichiometric composition to the Fe-rich side. At 427 °C, the thermal vacancy concentration in Fe-21 at.% Si is found to be by a factor of 30 lower than for 25 at.% Si [182]. Fe atom diffusion occurs by nearest-neighbor jumps on the Fe sublattice and is mediated by thermal vacancies. This explains the observation that Fe diffusion in the D0₃ ordered Fe₃Si is much faster and the corresponding activation enthalpy is considerably lower than in b.c.c. Fe or in disordered Fe-rich Fe–Si alloys [183].

With respect to the mechanical behavior of Fe–Si alloys, the embrittling effect of the occurrence of ordered intermetallic phases is known since long. Additions of up to about 10 at.% Si result in strengthening of the ferritic A2 material while still allowing plastic deformation at room temperature. Further increasing the Si content results in the occurrence of ordered B2 or D0₃ phase giving rise to an upward jump of the yield stress and a loss of ductility; see, e.g., Fig. 10.8, showing room-temperature compressive yield stress data taken from the systematic work of Lakso and Marcinkowski on Fe–Si alloys with up to 25 at.% Si (Fe₃Si) [184, 185]. D0₃ ordered Fe₃Si shows no ductility at room temperature and a low fracture strength of 400 MPa in tensile tests. On heating, the material shows a brittle-to-ductile transformation between 500 and 550 °C, and at 600 °C, a fair combination of strength (525 MPa) and ductility (4.5% strain to fracture) was observed [186].

The electrical resistivity of Fe approximately linearly increases with addition of Si in the disordered Fe solid solution. The occurrence of ordering results in a decrease with local resistivity minima for the compositions of the intermetallic phases Fe₃Si and Fe₅Si₃. The composition dependence of the room temperature resistivity is shown in Fig. 10.9 [187–189]. It should be mentioned that the data measured by Varga et al. [189] (15–34 at.% Si) were obtained from melt-spun material, which instead of being amorphous contained the ordered intermetallic phases Fe₃Si and Fe₅Si₃.

As the magnetic properties of Fe–Si alloys are of special importance for applications (see the respective section below), they were well investigated in the past with the first investigations dating back to the year 1900 [190]. Both the disordered α -Fe solid solution and the D0₃ ordered intermetallic phase Fe₃Si are

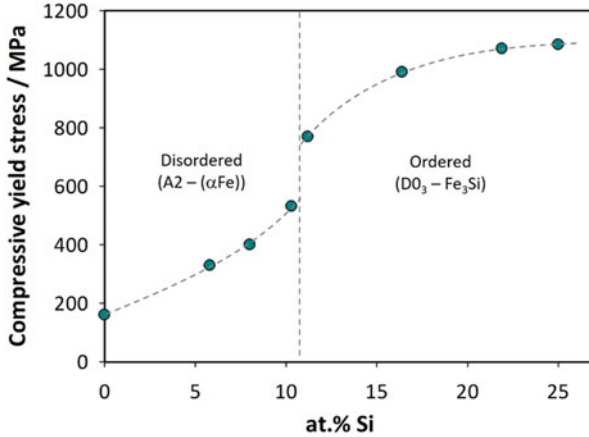


Fig. 10.8 Room-temperature compressive yield stresses of as-cast Fe–Si alloys. (Data taken from a figure shown in Ref. [179])

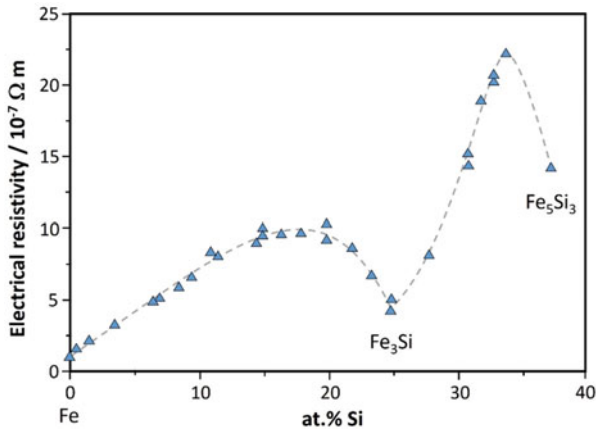


Fig. 10.9 Room-temperature electrical resistivity of Fe–Si alloys as a function of composition [187–189]. (Data taken from a figure shown in Ref. [189])

ferromagnetic with their Curie temperature and saturation magnetization decreasing continuously with increasing Si content; see, e.g., [191]. The Curie temperature T_C of stoichiometric Fe_3Si is 550 °C, and its mean magnetic moment μ amounts to 1.67 μ_B [192]. The high-temperature Fe-rich intermetallic phase Fe_5Si_3 can easily be metastably retained at room temperature, for example, as nanoparticles also showing ferromagnetic behavior [193]. For the Curie temperature of Fe_5Si_3 , values of 102–108 °C were reported [162, 193, 194]. In the Fe solid solution, Si addition effects an increase of magnetic permeability and electrical resistance as well as a decrease of the magnetic anisotropy, coercivity, and magnetostriction, where the latter approaches zero for a Si content of 12.1 at.% (6.5 wt.%); see, e.g., [195, 196].

The corrosion behavior of Fe_3Si is extraordinarily good; Fe_3Si is resistant even to boiling sulfuric and nitric acid [197, 198]. The good corrosion resistance of Fe_3Si is a result of the formation of a protecting SiO_2 layer. Studying the corrosion behavior in sulfuric acid, Yamaguchi [198] found that firstly the acid removes iron from the surface until a pure silicon layer remains, which then is oxidized to SiO_2 . According to Wasmuht [199], who studied the corrosion resistance in various acidic media for different Si contents, the existence of the single-phase, ordered intermetallic structure is a precondition for the excellent corrosion behavior with formation of protecting SiO_2 .

10.3.3 Processing and Applications

Huge amounts of silicon steels with typical Si contents of about 6 at.% (~3 wt.%) are produced every year by conventional casting and rolling procedures for application as electrical steels especially in electric motors and transformers. The beneficial effect of Si additions to Fe for improving the soft magnetic properties is well-known already since the seminal work of Hadfield and co-workers at the start of the last century [190]. Optimum soft magnetic behavior is reached for a Si content of 12.1 at.% (6.5 wt.%), where the magnetostriction decreases to zero resulting in noise-free power transmission and minimum core losses during cyclic magnetization processes; see, e.g., [195, 196]. Unfortunately, such an improvement of the magnetic properties is accompanied by a dramatic decrease in ductility starting at about 8 at.% Si (~4 wt.%), which makes conventional processing and specifically the required cold rolling of such alloys impossible. Besides segregation of Si to grain boundaries, the decisive factor is the occurrence of ordering leading to embrittlement of the material.

As the financial losses due to the application of material with non-optimized properties and high power losses are enormous, great efforts were put into finding suitable methods to produce Si-enriched Fe-6.5 wt.% Si electrical steel sheets either by trying to avoid ordering or by applying alternative processing methods for the ordered material. It should be noted that the occurrence of B2 or D0_3 (Fe_3Si) ordered regions per se is not the disqualifying criterion, but instead can be even beneficial for the magnetic properties, e.g., resulting in reduction of the coercivity [200]. The crucial point rather is the brittleness of these intermetallic phases. As commercial-scale production of Fe-6.5 wt.% Si sheets via a conventional cold rolling process is not possible, alternative production routes were explored including siliconizing of cold-rolled Fe-3 wt.% sheets by CVD (chemical vapor deposition) [201–203] or hot-dipping [204], spray-forming (based on atomization of a stream of the liquid alloy by Ar inert gas) [205, 206], direct powder rolling of iron and silicon powder mixtures with subsequent heat treatments [207], rapid quenching methods such as melt spinning [195, 200, 208], or ductilizing by microalloying with boron [209].

Today, Fe–Si alloys are still the most important soft magnetic material for electrical power conversion. Besides the conventional Fe-3 wt.% Si sheet cores,

so-called super cores with 6.5 wt.% Si produced via the CVD route were patented under the brand name JNEX[®] by JFE Steel Corp. [210, 211]. These non-oriented electrical steel sheet cores exhibit virtually zero magnetostriction resulting in low core losses and low noise in high-frequency applications. Competitors of sheet cores are compacted powder cores as the so-called Mega Flux core that was patented by Chang Sung Corp. [212, 213]. As the lack of ductility of Fe-6.5 wt.% Si prevents powder from being compacted, the Si content is adjusted to 4.5 wt.% in Mega Flux [213]. The properties and characteristics of the different core materials were compared in many studies revealing that the optimum choice strongly depends on the particular application [212–217].

The first Si-rich Fe–Si-based soft magnetic material, which already long time ago entered successfully into industrial applications, was so-called Sendust invented by Hakaru Masumoto and Tatsuji Yamamoto in 1937 [218]. Sendust, the name of which is a combination of Sendai and dust, is a ternary Fe-based alloy containing 9.6 wt.% Si and 5.4 wt.% Al and having the $D0_3$ Fe_3Si crystal structure. Due to its extreme brittleness, it is usually applied as sintered, partially or completely amorphous powder or rapidly quenched ribbons, but was also produced in sheet form through metal powder rolling techniques [219]. Sendust cores can have extremely high magnetic permeability with simultaneously low coercivity and as Sendust at the same time shows very good wear properties, it is used for magnetic recording heads [220, 221]. Composites consisting of Sendust flakes embedded in a polymer were produced for high-frequency applications in, e.g., mobile phones or personal computers to act as electromagnetic noise suppressor [222, 223]. Today, various composite powder cores are available with different standardized sizes and permeabilities, which can be combined to get new effective permeabilities [224]. Compared to the Fe–Si Mega Flux cores, Sendust cores show superior performance in transformers and inductors with respect to acoustic noise emission [225].

Due to its excellent corrosion resistance, castings of Fe_3Si are used since long as industrial components in contact with chemically aggressive media. An alloy with 25.2 at.% Si (14.5 wt.%) was developed and patented as “Duriron” by P.D. Schenck, W.E. Hall, and J.R. Pitman, who soon after (in 1912) incorporated the “During Casting Company” [226–228]. Duriron is not only corrosion resistant in inorganic and organic acidic environments but also in various alkaline solutions [199]. Its excellent corrosion behavior is comparable to that of noble metals, but as it is much cheaper, this material is extensively used in chemical industry since more than 100 years. The major drawback for production of parts from Fe_3Si is its extreme brittleness and hardness, which is why such parts can be only produced by casting.

With its good corrosion resistance, high hardness, and high electrical resistivity, Fe_3Si is also a candidate as protective surface coating, for example, on Fe–Si electrical steels. This was proven by Schneeweiss et al. [229] who successfully prepared an Fe_3Si coating by firstly CVD of a 1 μ m Si layer on Fe-3wt.%Si steel followed by some heat treatments that transformed the Si layer to a protective, 3–4- μ m-thick Fe_3Si coating.

Fe₃Si thin films are also good candidates for applications in microelectronics, e.g., as ferromagnetic electrode in spintronic devices utilizing the high spin polarization and high Curie temperature of Fe₃Si. Thin, epitaxial films were grown on semiconductor substrates such as GaAs [230, 231] or on SiO₂ for application as magnetic tunnel junctions [232, 233]. As a possible starting material for preparation of such thin layers, Fe₃Si nanoparticles (size approximately 5 nm) were successfully produced by a high-temperature chemical reduction method employing a reaction of silicon tetrachloride with iron pentacarbonyl [234].

10.4 Iron-Based Ferritic Superalloys

This chapter deals with ferritic iron-based alloys, where a disordered b.c.c. phase forms a coherent microstructure with an intermetallic phase. As the microstructures resemble those of the Ni-based superalloys, they have been termed ferritic superalloys. These alloys usually show high strength at elevated temperature and, therefore, recently have attracted much attention.

Because of lower costs, lower thermal expansion, and higher thermal conductivity, ferritic alloys are an interesting alternative to austenitic steels for high-temperature applications [235]. However, their poor creep resistance above 600 °C has limited their usage so far. Strengthening by coherent precipitates is an efficient method to obtain appreciable strength at high temperatures, as realized by the γ/γ' microstructures in superalloys. These superalloys were originally iron-based, but shifted to Ni and Co base already in the 1940s, and these alloys are still the backbone for applications at high temperatures [236, 237]. Strengthening the matrix by coherent NiAl precipitates is another method that has been successfully employed for maraging steels [238–240]. This concept has been recently refined to strengthening by coherent nanoprecipitates [241]. Also more recently f.c.c. + NiAl alloys with lamellar microstructures gained some interest because they show high strength and good ductility at room temperature [242]. In the following, ferrous materials other than steels with coherent microstructures are dealt with.

Specifically in many Fe–Al–X systems (X = Ni, Co, V, Ti . . .), miscibility gaps exist in which on cooling coherent microstructures of (α -Fe) + B2 (Fe,X)Al, (α -Fe) + L2₁ Heusler-type Fe₂AlX, or (Fe,X)Al + Fe₂AlX form. The three phases are crystallographically closely related to each other and have lattice constants quite close to each other (a_0 (α -Fe) \approx a_0 (Fe,X)Al \approx $\frac{1}{2}$ a_0 Fe₂AlX), and it is therefore that they readily form coherent microstructures. It has been shown that increased strength does not depend on whether the disordered or the intermetallic phase forms the precipitates [243], though alloy developments are preferentially aiming at precipitating the intermetallic phase. Microstructures can vary in dependence on the volume fractions from isolated precipitates to chessboard-like to maze-like [70]. The strength of the alloys will be determined by the size of the precipitates, width of the channels between them, and the coherency stresses. At least in some of the investigated systems, the precipitates form by spinodal decomposition, which gives

rise to second and third generations of precipitates. These fine-scaled precipitates have an additional strengthening effect but may also cause severe embrittlement at lower temperatures [70].

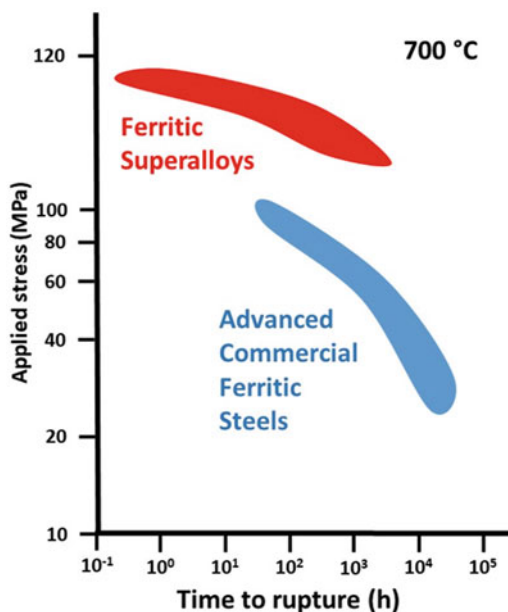
10.4.1 Alloy Developments

Initial alloy developments were based on the Fe–Al–X systems with Ni and Ti. Currently the focus is on Fe–Al–Ni–Ti–Cr alloys with minor additions of other elements [244]. By microstructural engineering the misfit between matrix and precipitates, i.e., the coherency stress, is optimized, and formation of sub-precipitates within the primary precipitates is employed for further strength increase [245]. These measures also help to avoid rapid coarsening which otherwise can be an issue [246]. A different approach to generate coherent microstructures is pursued in the Fe–Al–X systems with Nb and Ta. In these systems precipitation of the stable Laves phase is kinetically retarded, and a metastable Heusler phase forms instead [57]. The Heusler phase forms coherent microstructures with the matrix, which, dependent on temperature and composition, can be (α -Fe) or (Fe,X)Al. Though metastable, the coherent microstructures are stable for long time at elevated temperatures. Above 700–750 °C, the stable Laves phase will form, but as precipitation is primarily along grain boundaries, strength at high temperature can be maintained [73].

10.4.2 Properties

The strength of ferritic superalloys outperforms that of advanced Cr steels and matches that of Ni-based superalloys (Fig. 10.10). The yield strength at 800 °C varies between 100 and 300 MPa [70, 72, 73]. At 700 °C, secondary creep rates of 10^{-8} s^{-1} are observed at applied stresses between 90 and 200 MPa [72, 73, 247, 248], and the rate-determining deformation mechanisms have been intensively studied [243, 244, 247–250]. As the alloys are rather strong, they show only limited ductility at room temperature. It has been shown that ductility mainly depends on the volume fraction of precipitates [251, 252]. Specifically alloys with fine-scaled second- and third-generation precipitates can be rather brittle, and ductility may enhance after coarsening the fine precipitates through annealing [251, 253]. For sufficient corrosion resistance, the constituting phases must have an adequate content of Al plus Cr. Then they will show an excellent corrosion resistance like the iron aluminide alloys discussed in Sect. 10.2.

Fig. 10.10 Double logarithmic graph showing applied tensile stress against rupture life for advanced commercial steels (P92, P122, T91, T122, Cr12) in comparison to novel ferritic superalloys. (Figure adopted from Ref. [247])



10.4.3 Processing

Casting, forging, and additive manufacturing of ferritic superalloys have been demonstrated [121, 133]. Because of their high strength, forging must be performed at temperatures above the solvus. Forged and additive processed alloys showed comparable strength as their as-cast counterparts but partly increased ductility [133, 136]. As these alloys are still under development, their processing/property relationships must be still evaluated, and no applications have been realized yet.

10.5 Iron-Based Alloys with TCP Phases

Laves phases and other topological close-packed (TCP) phases are common precipitates in steels. They are very strong phases, and therefore they have been considered for strengthening steels already long time ago, either as additional precipitates to carbides or in C-free alloys and low-carbon steels, e.g., maraging steels [3, 254–256]. However, it has been found that they precipitate preferentially at grain boundaries, where they do not contribute much to strengthening but instead induce formation of cavities and cause embrittlement [6, 257]. They are also unwanted, because after formation they tend to rapidly coarsen, thereby extracting the elements responsible for solid solution hardening like W and Mo from the matrix [8, 257–260]. However, reports are varying, and if compositions are carefully

adjusted, Laves and other TCP phases may be beneficial in attaining strength at high temperature [261, 262].

The key for gaining strength at high temperatures by TCP precipitates is their distribution. Early attempts used fine precipitates of spheroidized Laves phase [254]. A new concept is to precipitate the TCP phases as more or less continuous film along the grain boundaries. The resulting steels are very strong, and it has been demonstrated that though the TCP phases are rather brittle as monolithic phase, the films show good mechanical behavior, i.e., they do not show cracking after plastic deformation [263, 264]. Both ferritic and austenitic steels are currently under development.

10.5.1 Ferritic(–Martensitic) TCP Steels

Strengthening ferritic 9–12 wt.% Cr steels by Laves phase and other TCP precipitates has been investigated for quite some time. Usually elements such as Nb, W, and Mo are added to provoke their formation. In general it is found that the Laves phase, which precipitates during creep, initially increases the creep resistance. However, due to rapid coarsening, the creep rate may increase again after some time [258].

More recently, specifically Cr-rich steels are developed which gain their strength from TCP phases. 15 wt.% Cr steels containing Laves phase and μ phase (and χ phase) show a superior creep resistance due to fine precipitation of the TCP phases in the matrix [265].

Crofer 22H is a ferritic steel strengthened by Laves precipitates within the $\alpha(\text{Fe,Cr})$ matrix [266]. It was developed as a high strength steel for interconnections in solid oxide fuel cells (SOFCs). Compared to the precipitate-free Cr steel JS-3, it shows a much better creep resistance due to solid solution hardening and the precipitation of micron-sized $\text{Fe}_2\text{Nb(W)}$ Laves phase precipitates. The oxidation behavior does not deteriorate by the addition of Nb, W, and Si, and this steel has a total elongation of >20% at room temperature [266]. Further optimization of the microstructure showed that distributing the Laves phase at the grain boundary is very effective to prevent coarsening of the ferritic matrix as the Laves phase itself coarsens only very slowly [267, 268]. The concept is further elaborated in the development of HiperFer, another high chromium-containing steel for highly efficient steam power plants that has a better steam oxidation resistance and higher strength than P92 [263, 269].

10.5.2 Austenitic TCP Steels

Based on the design concept of grain boundary precipitation strengthening, Takeyama et al. developed a highly creep-resistant but still sufficiently ductile steel of composition Fe-30Cr-20Ni-2Nb (in at.%) [270, 271]. This steel has a

three-dimensional network of the Fe_2Nb Laves phase precipitated as a film of $<1\ \mu\text{m}$ thickness on the austenite grain boundaries and additional fine nanometer-sized plates of Ni_3Nb inside the austenite grains [264]. It has been shown that the properties crucially depend on the area fraction of the grain boundaries covered by Laves phase, i.e., that strength increases and ductility decreases with increasing fraction of Laves phase. An alloy with about 90% coverage of the grain boundaries attained a creep life of 880 h at 700 °C and 140 MPa [270]. However, crack formation neither inside the Laves phase nor at the Laves/ γ -Fe interface was observed [264]. The steel has a good corrosion resistance in steam in that it readily forms a protective Cr_2O_3 scale [272]. Main application of the steel could be in advanced thermal power plants.

10.6 Summary and Future Outlook

In view of their potential to replace high-alloyed steels or even Co- or Ni-based superalloys, iron-based intermetallic materials are an inexpensive alternative. As they are iron based, they can be produced using equipment readily available in iron and steel companies. Though these materials are not “another steel,” at least part of the processing can be based on experience gained from the processing of cast iron or steels. Their limited ductility is still adequate for many applications. It may cause a bit more time-consuming machining, but near net shape processing, which has been successfully demonstrated, can substantially reduce costs for machining.

Their excellent strength-to-weight ratio, i.e., their specific strength, their partly outstanding corrosion resistance, and high wear resistance, opens up new possibilities to use these iron-based materials under demanding conditions, otherwise only bearable by Co- and Ni-based superalloys. In view of these properties, iron-based intermetallic materials offer an increased lifetime combined with reduced energy consumption. Iron, aluminum, and silicon are the most abundant elements, and the materials discussed in this chapter need no or little additional alloying. Therefore, besides economic considerations, with increasing lack of strategic elements, these materials for sure will get more attention in the future.

References

1. G.E.R. Schulze, *Metallphysik* (Akademie-Verlag, Berlin, 1967), pp. 1–76
2. S. Floreen, The physical metallurgy of maraging steels. *Metall. Rev.* **13**, 115–128 (1968)
3. V.K. Vasudevan, S.J. Kim, C.M. Wayman, Precipitation reactions and strengthening behavior in 18 wt pct nickel maraging steels. *Metal. Trans.* **21A**(10), 2655–2668 (1990)
4. D. Raabe et al., Designing ultrahigh strength steels with good ductility by combining transformation induced plasticity and martensite aging. *Adv. Eng. Mater.* **11**(7), 547–555 (2009)

5. S. Floreen, An examination of chromium substitution in stainless steels. *Metal. Trans.* **13A**(11), 2003–2013 (1982)
6. K. Asakura, Y. Kobuchi, T. Fujita, Embrittlement factors in high-Cr ferritic heat resisting steels. *Tetsu-to-hagane* **75**(7), 1209–1216 (1989)
7. D.J. Thoma, Intermetallics: Laves phases, in *Encyclopedia of Materials: Science and Technology*, ed. by K. H. J. Buschow et al., (Elsevier, Amsterdam, 2001), pp. 4205–4213
8. P.J. Ennis et al., Microstructural stability and creep rupture strength of the martensitic steel P92 for advanced power plant. *Acta Mater.* **45**(12), 4901–4907 (1997)
9. M. Palm, F. Stein, G. Dehm, Iron aluminides. *Ann. Rev. Mater. Res.* **49**, 297–326 (2019)
10. M. Hansen, K. Anderko, Aluminium-iron, in *Constitution of Binary Alloys*, ed. by M. Hansen, K. Anderko, (McGraw Hill Book Company, New York, 1958), pp. 90–95
11. F. Stein, M. Palm, Re-determination of transition temperatures in the Fe-Al system by differential thermal analysis. *Int. J. Mat. Res.* **98**(7), 580–588 (2007)
12. X. Li et al., The Al-rich part of the Fe-Al phase diagram. *J. Phase Equil. Diffus.* **37**(2), 162–173 (2016)
13. R.A. Hadfield, Aluminium-steel. *J. Iron Steel Inst.* **2**, 161–230 (1890)
14. W.J. Keep, Aluminum in cast iron. *Trans. AIME* **18**, 102–122 (1890)
15. H.F. Durnenko, Aluminevy cugun (Cugal). *Liteiscik* **7** (1934)
16. J.W. Bampfylde, *B.C.I.R.A. Improvements in and Relating to the Manufacture of Cast Iron Alloys* (UK, 1938)
17. J.F. Nachman, W.J. Buehler, *The Fabrication and Properties of 16-ALFENOL – A Non-strategic Aluminum-Iron Alloy* (Naval Ordnance Laboratory, 1953), pp. 1–23
18. W.J. Buehler, C.G. Dalrymple, Coming: better thermenol alloys. *Met. Prog.* **73**(5), 78–81 (1958)
19. E.R. Morgan, V.F. Zackay, Ductile iron aluminum alloys. *Met. Prog.* **68**(10), 126–128 (1955)
20. W.J. Lepkowski, J.W. Holladay, *The Present State of Development of Iron-Aluminum-Base Alloys* (Battelle Memorial Institute, 1957), pp. 1–39
21. R. Brooks, A. Volio, *Iron-Aluminum Alloy Systems, Part 14 Welding of Iron Aluminum Alloys* (Wright Air Development Center; Wright Patterson Airforce Base, OH, USA, 1959), pp. 1–24
22. W. Chubb et al., *Constitution, Metallurgy, and Oxidation Resistance of Iron-Chromium-Aluminum Alloys* (Battelle Memorial Institute, 1958), pp. 1–104
23. J.W. Holladay, *Review of Developments in Iron-Aluminum-Base Alloys* (Battelle Memorial Institute, 1961), pp. 1–57
24. M.A. Plesinger, Les nouveaux alliages refractaires developpes en Tchecoslovaquie. *Fonderie* **157**(2), 75–88 (1959)
25. P. Kratochvil, The history of the search and use of heat resistant Pyroferal alloys based on FeAl. *Intermetallics* **16**(4), 587–591 (2008)
26. Z. Tyszko, Fontes a haute teneur en aluminium. *Fonderie* **278**, 221–233 (1969)
27. J.F. Nachman, E.R. Duffy, Effect of alloying additions on sea water corrosion resistance of iron-aluminum base alloys. *Corrosion* **30**(10), 357–365 (1974)
28. G. Culbertson, C.S. Kortovich, *Development of Iron Aluminides* (AF Wright Aeronautical Laboratories, 1986), pp. 1–149
29. R.G. Bordeau, *Development of Iron Aluminides* (AF Wright Aeronautical Laboratories, 1987), pp. 1–264
30. B. King, *Dispersion Strengthening of Iron Aluminium Base Alloys: A Feasibility Study* (Oak Ridge National Laboratory, 1960), pp. 1–45
31. C.G. McKamey, Iron aluminides, in *Physical Metallurgy and Processing of Intermetallic Compounds*, ed. by N. S. Stoloff, V. K. Sikka, (Chapman & Hall, New York, 1996), pp. 351–391
32. C.G. McKamey et al., A review of recent developments in Fe₃Al-based alloys. *J. Mater. Res.* **6**(8), 1779–1805 (1991)
33. S.C. Deevi, V.K. Sikka, Nickel and iron aluminides: an overview on properties, processing, and applications. *Intermetallics* **4**(5), 357–375 (1996)

34. C.T. Liu et al., Recent advances in B2 iron aluminide alloys: deformation, fracture and alloy design. *Mater. Sci. Eng. A* **258**, 84–98 (1998)
35. P.F. Tortorelli, K. Natesan, Critical factors affecting the high-temperature corrosion performance of iron aluminides. *Mater. Sci. Eng. A* **258**, 115–125 (1998)
36. S. Revol, R. Baccino, F. Moret, *Industrial Applications of FeAl40Grade3, A High Specific Properties Iron Aluminides*. in *EUROMAT99* (Wiley-VCH, Weinheim, 2000)
37. R.G. Baligidad, A. Radhakrishna, Effect of hot rolling and heat treatment on structure and properties of high carbon Fe-Al alloys. *Mater. Sci. Eng. A* **308**, 136–142 (2001)
38. R.G. Baligidad, V.V. Satya Prasad, A. Sambasiva Rao, Effect of Ti, W, Mn, Mo and Si on microstructure and mechanical properties of high carbon Fe-10.5 wt-% Al alloy. *Mater. Sci. Technol.* **23**(5), 613–619 (2007)
39. M. Palm, Fe-Al materials for structural applications at high temperatures: current research at MPIE. *Int. J. Mater. Res.* **100**(3), 277–287 (2009)
40. D. Paris, P. Lesbats, J. Levy, An investigation of the distribution of vacancies in an ordered Fe-Al alloy by field ion microscopy. *Scr. Metall.* **9**, 1373–1378 (1975)
41. M. Kogachi, T. Haraguchi, Quenched-in vacancies in B2-structured intermetallic compound FeAl. *Mater. Sci. Eng. A* **230**(1-2), 124–131 (1997)
42. Y. Yang, I. Baker, The influence of vacancy concentration on the mechanical behavior of Fe-40Al. *Intermetallics* **6**, 167–175 (1998)
43. G. Hasemann, J.H. Schneibel, E.P. George, Dependence of the yield stress of Fe₃Al on heat treatment. *Intermetallics* **21**(9), 56–61 (2012)
44. G. Dlubek, O. Brümmer, B. Möser, The recovery of quenched-in vacancies in Fe-Al (6.3 to 28.3 at.%) alloys studied by positron annihilation. *Cryst. Res. Technol.* **17**(8), 951–961 (1982)
45. I. Baker, D.J. Gaydos, Flow and fracture of Fe-Al. *Mater. Sci. Eng.* **96**, 147–158 (1987)
46. J.T. Guo et al., Discovery and study of anomalous yield strength peak in FeAl alloy. *Scr. Metall. Mater.* **29**(6), 783–785 (1993)
47. K. Yoshimi, S. Hanada, M.H. Yoo, Yielding and plastic flow behavior of B2-type Fe-39.5 mol.% single crystals in compression. *Acta Metall. Mater.* **43**(11), 4141–4151 (1995)
48. D.G. Morris, M.A. Munoz-Morris, The stress anomaly in FeAl-Fe₃Al alloys. *Intermetallics* **13**(12), 1269–1274 (2005)
49. D.G. Morris, M.A. Munoz-Morris, A re-examination of the pinning mechanisms responsible for the stress anomaly in FeAl intermetallics. *Intermetallics* **18**(7), 1279–1284 (2010)
50. E.P. George, I. Baker, Thermal vacancies and the yield strength anomaly of FeAl. *Intermetallics* **6**, 759–763 (1998)
51. D.J. Schmatz, R.H. Bush, Elevated temperature yield effect in iron-aluminum. *Acta Metall.* **16**(2), 207–217 (1968)
52. J.H. Song, T.K. Ha, Y.W. Chang, Anomalous temperature dependence of flow stress in a Fe₃Al alloy. *Scr. Mater.* **42**(3), 271–276 (2000)
53. C.T. Liu, E.H. Lee, C.G. McKamey, An environmental effect as the major cause for room-temperature embrittlement in FeAl. *Scr. Metall.* **23**, 875–880 (1989)
54. N.S. Stoloff et al., Environmental embrittlement of Fe₃Al alloys under monotonic and cyclic loading, in *Processing, Properties, and Applications of Iron Aluminides*, (TMS, Warrendale, 1994)
55. M. Zamanzade, A. Barnoush, An overview of the hydrogen embrittlement of iron aluminides. *Proc. Mater. Sci.* **3**, 2016–2023 (2014)
56. D. Hardwick, G. Wallwork, Iron-aluminium alloys: a review of their feasibility as high-temperature materials. *Rev. High-Temp. Mater.* **4**(1), 47–74 (1978)
57. M.G. Mendiratta et al., A review of recent developments in iron aluminides. *Mater. Res. Soc. Symp. Proc.* **81**, 393–404 (1987)
58. D.G. Morris, M.A. Morris, Strengthening at intermediate temperatures in iron aluminides. *Mater. Sci. Eng. A* **239**, 23–38 (1997)
59. D.G. Morris, Possibilities for high-temperature strengthening in iron aluminides. *Intermetallics* **6**, 753–758 (1998)

60. A. Bahadur, Enhancement of high temperature strength and room temperature ductility of iron aluminides by alloying. *Mater. Sci. Technol.* **19**, 1627–1634 (2003)
61. M. Palm, Concepts derived from phase diagram studies for the strengthening of Fe-Al-based alloys. *Intermetallics* **13**(12), 1286–1295 (2005)
62. F. Stein, A. Schneider, G. Frommeyer, Flow stress anomaly and order-disorder transitions in Fe₃Al-based Fe-Al-Ti-X alloys with X = V, Cr, Nb, or Mo. *Intermetallics* **11**, 71–82 (2003)
63. D. Risanti et al., Dependence of the brittle-to-ductile transition temperature (BDTT) on the Al content of Fe-Al alloys. *Intermetallics* **13**(12), 1337–1342 (2005)
64. A. Schneider et al., Microstructures and mechanical properties of Fe₃Al-based Fe-Al-C alloys. *Intermetallics* **13**(12), 1322–1331 (2005)
65. L. Falat et al., Mechanical properties of Fe-Al-M-C (M = Ti, V, Nb, Ta) alloys with strengthening carbides and Laves phase. *Intermetallics* **13**(12), 1256–1262 (2005)
66. R. Krein et al., Microstructure and mechanical properties of Fe₃Al-based alloys with strengthening boride precipitates. *Intermetallics* **15**(9), 1172–1182 (2007)
67. M. Palm, G. Sauthoff, Deformation behaviour and oxidation resistance of single-phase and two-phase L₂₁-ordered Fe-Al-Ti alloys. *Intermetallics* **12**, 1345–1359 (2004)
68. R. Krein, M. Palm, The influence of Cr and B additions on the mechanical properties and oxidation behaviour of L₂₁-ordered Fe-Al-Ti-based alloys at high temperatures. *Acta Mater.* **56**(10), 2400–2405 (2008)
69. X. Li, P. Prokopcakova, M. Palm, Microstructure and mechanical properties of Fe-Al-Ti-B alloys with additions of Mo and W. *Mater. Sci. Eng. A* **611**, 234–241 (2014)
70. C. Stallybrass, G. Sauthoff, Ferritic Fe-Al-Ni-Cr alloys with coherent precipitates for high-temperature application. *Mater. Sci. Eng. A* **387–389**, 985–990 (2004)
71. C. Stallybrass, *The Precipitation Behaviour and Mechanical Properties of Novel Fe-Al-Ni-Cr Alloys with Coherent Precipitates* (Shaker Verlag, Aachen, 2008), pp. 1–194
72. R. Krein, M. Palm, M. Heilmaier, Characterisation of microstructures, mechanical properties, and oxidation behaviour of coherent A₂ + L₂₁ Fe-Al-Ti alloys. *J. Mater. Res.* **24**(11), 3412–3421 (2009)
73. D.D. Risanti, G. Sauthoff, Microstructures and mechanical properties of Fe-Al-Ta alloys with strengthening Laves phase. *Intermetallics* **19**, 1727–1736 (2011)
74. M. Eumann, M. Palm, G. Sauthoff, Alloys based on Fe₃Al or FeAl with strengthening Mo₃Al precipitates. *Intermetallics* **12**(6), 625–633 (2004)
75. T. Doucak, K.S. Kumar, Formation and stability of refractory metal diborides in an Fe₃Al matrix. *Intermetallics* **7**, 765–777 (1999)
76. F. Stein, M. Palm, G. Sauthoff, Mechanical properties and oxidation behaviour of two-phase iron aluminium alloys with Zr(Fe,Al)₂ Laves phase or Zr(Fe,Al)₁₂ τ₁ phase. *Intermetallics* **13**(12), 1275–1285 (2005)
77. P. Prokopcakova, M. Svec, M. Palm, Microstructural evolution and creep of Fe-Al-Ta alloys. *Int. J. Mater. Res.* **107**(5), 396–405 (2016)
78. I. Ohnuma et al., Ordering and phase separation in the b.c.c. phase of the Fe-Al-Ti system. *Acta Mater.* **46**(6), 2083–2094 (1998)
79. C.G. McKamey et al., Effects of alloying additions on the microstructures, mechanical properties and weldability of Fe₃Al-based alloys. *Mater. Sci. Eng. A* **174**(1), 59–70 (1994)
80. R. Balasubramaniam, Alloy development to minimize room temperature hydrogen embrittlement in iron aluminides. *J. Alloys Compd.* **253–254**, 148–151 (1997)
81. D.G. Morris, M.A. Morris-Munoz, The influence of microstructure on the ductility of iron aluminides. *Intermetallics* **7**(10), 1121–1129 (1999)
82. K. Vedula, FeAl and Fe₃Al, in *Intermetallic Compounds*, Practice, ed. by J. H. Westbrook, R. L. Fleischer, vol. 2, (Wiley, Chichester, 1995), pp. 199–209
83. N.S. Stoloff, D.A. Alven, C.G. McKamey, An overview of Fe₃Al alloy development with emphasis on creep and fatigue, in *International Symposium on Nickel and Iron Aluminides: Processing, Properties, and Applications*, (ASM International, 1997)
84. A. Tonneau, M. Gerland, G. Henaff, Environment-sensitive fracture of iron aluminides during cyclic crack growth. *Metall. Mater. Trans. A* **32**(9), 2345–2356 (2001)

85. G.E. Fuchs, N.S. Stoloff, Effects of temperature, ordering and composition on high cycle fatigue of polycrystalline Fe₃Al. *Acta Metall.* **36**(5), 1381–1387 (1988)
86. H.Y. Yasuda, A. Behgozin, Y. Umakoshi, Fatigue behavior of Fe-48.at% Al polycrystals with B2 structure at high temperatures. *Scr. Mater.* **40**(2), 203–207 (1999)
87. M. Johnson et al., The resistance of nickel and iron aluminides to cavitation erosion and abrasive wear. *Wear* **140**, 279–289 (1990)
88. A. Magnee, Generalized law of erosion: application to various alloys and intermetallics. *Wear* **181–183**, 500–510 (1995)
89. J. Xia, Thermal oxidation treatment of iron aluminide for improved tribological properties. *Surf. Eng.* **21**(1), 6–11 (2005)
90. J.P. Tu, M.S. Liu, Wet abrasive wear of ordered Fe₃Al alloys. *Wear* **209**, 31–36 (1997)
91. Y.S. Kim, J.H. Song, Y.W. Chang, Erosion behavior of Fe-Al intermetallic alloys. *Scr. Mat.* **36**(7), 829–834 (1997)
92. H. Hindam, D.P. Whittle, Microstructure, adhesion and growth kinetics of protective scales on metals and alloys. *Oxid. Met.* **18**, 245–284 (1982)
93. P. Tomaszewicz, G. Wallwork, Iron-aluminium alloys: a review of their oxidation behaviour. *Rev. High-Temp. Mater.* **4**(1), 75–104 (1978)
94. F.H. Stott, K.T. Chuah, L.B. Bradley, Oxidation-sulphidation of iron aluminides at high temperature. *Mater. Corros.* **47**, 695–700 (1996)
95. J. Klöwer, High-temperature corrosion behavior of iron aluminides and iron-aluminum-chromium alloys. *Mater. Corros.* **47**, 685–694 (1996)
96. A. Schneider, J. Zhang, Metal dusting of ferritic Fe-Al-M-C (M = Ti, V, Nb, Ta) alloys in CO-H₂-H₂O gas mixtures at 650 °C. *Mater. Corros.* **54**(10), 778–784 (2003)
97. D.J. Duquette, Corrosion of intermetallic compounds, in *Intermetallic Compounds*, Principles, ed. by J. H. Westbrook, R. L. Fleischer, vol. 1, (Wiley, Chichester, 1995), pp. 965–975
98. V. Shankar Rao, A review of the electrochemical corrosion behaviour of iron aluminides. *Electrochim. Acta* **49**, 4533–4542 (2004)
99. J.G. Kim, R.A. Buchanan, Pitting and crevice corrosion of iron aluminides in a mild acid-chloride solution. *Corrosion* **50**(9), 658–668 (1994)
100. J. Peng et al., Influence of Al content and pre-oxidation on the aqueous corrosion resistance of binary Fe-Al alloys in sulphuric acid. *Corros. Sci.* **149**, 123–132 (2019)
101. M. Palm, R. Krieg, Neutral salt spray tests on Fe-Al and Fe-Al-X. *Corros. Sci.* **64**, 74–81 (2012)
102. S. Frangini, Corrosion behavior of AISI 316L stainless steel and ODS FeAl aluminide in eutectic Li₂CO₃-K₂CO₃ molten carbonates under flowing CO₂-O₂ gas mixtures. *Oxid. Met.* **53**(1/2), 139–156 (2000)
103. M. Amaya et al., High temperature corrosion performance of FeAl intermetallic alloys in molten salts. *Mater. Sci. Eng. A* **349**, 12–19 (2003)
104. V. Marx, M. Palm, Oxidation of Fe-Al Alloys (5–40 at.% Al) at 700 and 900 °C. *Mat. Sci. Forum* **879**, 1245–1250 (2017)
105. D. Vogel et al., Corrosion behaviour of Fe-Al(-Ti) alloys in steam. *Intermetallics* **18**, 1375–1378 (2010)
106. W.J. Lepkowski, J.W. Holladay, *The Present State of Development of Iron-Aluminum-Base Alloys* (Battelle Memorial Institute, 1957), pp. 1–39
107. C. Sykes, J.W. Bampfyld, The physical properties of iron-aluminium alloys. *J. Iron Steel Inst.* **130**, 389–418 (1934)
108. Y.D. Huang et al., Preparation and mechanical properties of large-ingot Fe₃Al-based alloys. *J. Mater. Proc. Technol.* **146**, 175–180 (2004)
109. V.K. Sikka et al., Melting and casting of FeAl-based alloy. *Mater. Sci. Eng. A* **258**, 229–235 (1998)
110. A. Radhakrishna, R.G. Baligidad, D.S. Sarma, Effect of carbon on structure and properties of FeAl based intermetallic alloy. *Scr. Mater.* **45**, 1077–1082 (2001)
111. T. Itoi et al., Preparation of recycle-typed Fe₃Al alloy and its application for cutting tool materials. *Intermetallics* **18**(7), 1396–1400 (2010)

112. D.F.L. Borges, D.C.R. Espinosa, C.G. Schön, Making iron aluminides out of scrap. *J. Mater. Res. Technol.* **3**(2), 101–106 (2014)
113. K. Matsuura, Y. Watanabe, Y. Hirashima, Use of recycled steel machining chips and aluminum can shreds for synthesizing iron aluminide intermetallic alloys. *ISIJ Int.* **44**(7), 1258–1262 (2004)
114. B.H. Rabin, R.N. Wright, Synthesis of iron aluminides from elemental powders: reaction mechanisms and densification behavior. *Metall. Trans. A* **22**(2), 277–286 (1991)
115. E. Godlewska et al., FeAl materials from intermetallic powders. *Intermetallics* **11**(4), 307–312 (2003)
116. S. Paris et al., Spark plasma synthesis from mechanically activated powders: a versatile route for producing dense nanostructured iron aluminides. *Scr. Mater.* **50**(5), 691–696 (2004)
117. D.G. Morris, M.A. Munoz-Morris, Recent developments toward the application of iron aluminides in fossil fuel technologies. *Adv. Eng. Mater.* **13**(1-2), 43–47 (2011)
118. J.R. Blackford et al., Production of iron aluminides by strip casting followed by cold rolling at room temperature. *Scr. Mat.* **34**(10), 1595–1600 (1996)
119. O. Flores et al., Forging of FeAl intermetallic compounds, in *Processing, Properties and Applications of Iron Aluminides*, ed. by J. H. Schneibel, M. A. Crimp, (TMS, 1994), pp. 31–38
120. D.G. Morris, M.A. Munoz-Morris, High creep strength, dispersion-strengthened iron aluminide prepared by multidirectional high-strain forging. *Acta Mater.* **58**(10), 6080–6089 (2010)
121. P. Janschek et al., Forging of steam turbine blades with an Fe₃Al-based alloy. *Mater. Res. Soc. Symp. Proc.* **1128**, 47–52 (2009)
122. J.F. Nachman, W.J. Buehler, 16 percent aluminum-iron alloy cold rolled in the order-disorder temperature range. *J. Appl. Phys.* **25**(3), 307–313 (1954)
123. J.R. Blackford et al., Effect of process variables on tensile properties of ingot processed versus strip cast iron aluminides. *Mater. Sci. Technol.* **14**(11), 1132–1138 (1998)
124. C. Testani et al., FeAl intermetallics and applications: an overview, in *International Symposium on Nickel and Iron Aluminides: Processing, Properties, and Applications*, ed. by S. C. Deevi et al., (ASM International, Cincinnati, 1997), pp. 213–222
125. D. Kuc, G. Niewielski, I. Bednarczyk, The influence of thermomechanical treatment on structure of FeAl intermetallic phase-based alloys. *JAMME* **29**(2), 123–130 (2008)
126. I. Schindler et al., Forming of cast Fe – 45 at.% Al alloy with high content of carbon. *Intermetallics* **18**, 745–747 (2010)
127. S.C. Deevi et al., Processing and properties of FeAl sheets obtained by roll compaction and sintering of water atomized powders, in *High-temperature Ordered Intermetallic Alloys VIII*, (MRS, Warrendale, Boston, 1999)
128. S. Strothers, K. Vedula, Hot extrusion of B2 iron aluminide powders. *Prog. Powder Metall.* **43**, 597–610 (1987)
129. B. Kad et al., Optimization of high temperature hoop creep response in ODS-Fe₃Al tubes, in *17th Annual Conference on Fossil Energy Materials*, ed. by R. R. Judkins, (United States. Dept. of Energy. Office of Scientific and Technical Information, Baltimore, 2003), pp. 1–10
130. V.K. Sikka, S. Viswanathan, C.G. McKamey, Development and commercialization status of Fe₃Al-based intermetallic alloys, in *Structural Intermetallics*, (TMS, Seven Springs, 1993)
131. T. Durejko, M. Lazinska, W. Przetakiewicz, Manufacturing of Fe₃Al based materials using LENS method. *Inzyniera Materialowa (Inz. Mater.)* **35**(5), 353 (2012)
132. B. Song et al., Fabrication and microstructure characterization of selective laser-melted FeAl intermetallic parts. *Surf. Coat. Technol.* **206**(22), 4704–4709 (2012)
133. A. Michalcová et al., Laser additive manufacturing of iron aluminides strengthened by ordering, borides or coherent Heusler phase. *Mater. Des.* **116**, 481–494 (2016)
134. T. Durejko et al., Thin wall tubes with Fe₃Al/SS316L graded structure obtained by using laser engineered net shaping technology. *Mater. Des.* **63**, 766–774 (2014)
135. G. Rolink et al., Laser metal deposition and selective laser melting of Fe–28 at.% Al. *J. Mater. Res.* **29**(17), 2036–2043 (2014)

136. P. Hanus et al., Mechanical properties of a forged Fe–25Al–2Ta steam turbine blade. *Intermetallics* **18**, 1379–1384 (2010)
137. J. Konrad et al., Hot deformation behavior of a Fe₃Al-binary alloy in the A2 and B2-order regimes. *Intermetallics* **13**(12), 1304–1312 (2005)
138. N. Cinca, J.M. Guilemany, Thermal spraying of transition metal aluminides: an overview. *Intermetallics* **24**, 60–72 (2012)
139. N. Cinca, C.R.C. Lima, J.M. Guilemany, An overview of intermetallics research and application: status of thermal spray coatings. *J. Mater. Res. Technol.* **2**(1), 75–86 (2013)
140. B. Denkena, H.K. Tönshoff, D. Boehnke, An assessment of the machinability of iron-rich iron-aluminium alloys. *Steel Res. Int.* **76**(2/3), 261–264 (2005)
141. J. Köhler, A. Moral, B. Denkena, Grinding of iron-aluminides. *Proc. CIRP* **9**, 2–7 (2013)
142. S.A. David et al., Welding of iron aluminides. *Weld. J.* **68**(9), 372s–381s (1989)
143. M.L. Santella, An overview of the welding of Ni₃Al and Fe₃Al alloys, in *International Symposium on Nickel and Iron Aluminides: Processing, Properties, and Applications*, ed. by S. C. Deevi et al., (ASM Int.: Proc. Materials Week, Cincinnati, 1997), pp. 321–327
144. P.D. Sketchley, P.L. Threadgill, I.G. Wright, Rotary friction welding of an Fe₃Al based ODS alloy. *Mater. Sci. Eng. A* **329–331**, 756–762 (2002)
145. Z. Eminger, Beitrag zur Frage der Herstellung von Gußstücken aus der Eisen-Aluminium-Legierung “Pyroferal”. *Freiberger Forschungshefte* **B 24-I**, 121–144 (1957)
146. J. Cebulski, Application of FeAl intermetallic phase matrix based alloys in the turbine components of a turbo charger. *Metalurgija* **54**(1), 154–156 (2015)
147. P.J. Blau, H.M. Meyer III, Characteristics of wear particles produced during friction tests of conventional and unconventional disc brake materials. *Wear* **255**, 1261–1269 (2003)
148. F. Moszner et al., Application of iron aluminides in the combustion chamber of large bore 2-stroke marine engines. *Metals* **2019**(9), 847–857 (2019)
149. S Series PSS[®] Filter Elements Data Sheet, in Element Data Sheet E20c, P. Corporation, pp. 1–3.
150. C.G. McKamey et al., Characterization of field-exposed iron aluminide hot gas filters, in *5th International Symposium on Gas Cleaning at High Temperature*, (Morgantown, 2002), pp. 18–20
151. O. Kubaschewski, *Iron – Binary Phase Diagrams* (Springer, Berlin, 1982), p. 185
152. H. Okamoto (ed.), *Desk Handbook Phase Diagrams for Binary Alloys*, 2nd edn. (Materials Park, ASM International, 2010), p. 855
153. I. Ohnuma et al., Experimental and thermodynamic studies of the Fe-Si binary system. *ISIJ Int.* **52**(4), 540–548 (2012)
154. S. Cui, I.-H. Jung, Critical reassessment of the Fe-Si system. *Calphad* **56**, 108–125 (2017)
155. G. Inden, W. Pitsch, Ordering transitions in body centered cubic iron silicon alloys – II. Experimental determination of the atomic configurations. *Z. Metallkd.* **63**, 253–258 (1972)
156. G. Schlatter, G. Inden, W. Pitsch, Ordering transitions in body centered cubic iron silicon alloys – IV. Theory with simultaneous consideration of chemical and magnetic interactions. *Z. Metallkd.* **65**, 94–100 (1974)
157. G. Schlatter, W. Pitsch, Ordering transitions in body centered cubic iron silicon alloys – V. Electronmicroscopic observations. *Z. Metallkd.* **66**, 660–668 (1975)
158. G. Schlatter, W. Pitsch, Ordering transitions in body centered cubic iron silicon alloys – VI. Comparison between theory and experiment. *Z. Metallkd.* **67**, 462–466 (1976)
159. K. Hilfrich et al., Revision of the Fe-Si-phase diagram: no B2-phase for 7.6 At.% c_{Si} <math>< 10.2</math> At.%. *Scr. Metall. Mater.* **24**(1), 39–44 (1990)
160. F. González, Y. Houbaert, A review of ordering phenomena in iron-silicon alloys. *Rev. Metal. (Madrid, Spain)* **49**(3), 178–199 (2013)
161. H. Kudielka, Die Kristallstruktur von Fe₂Si, ihre Verwandtschaft zu den Ordnungsstrukturen des α -(Fe,Si)-Mischkristalls und zur Fe₅Si₃-Struktur. *Z. Kristallogr. Crystal. Mater.* **145**(3–4), 177–189 (1977)
162. P. Lecocq, A. Michel, Etude magnétique et structurale de phases semi-métalliques. Les composés ferromagnétiques de structure D8₅, Mn₅Ge₃ et Fe₅Si₃. *Bull. Soc. Chim. Fr.* **1965**, 307–310 (1965)

163. F. Wever, H. Möller, Über den Kristallbau des Eisensilizides FeSi. *Z. Kristallogr.* **75**, 362–365 (1930)
164. C. Le Corre, J.M. Genin, Transformation mechanisms of the $\alpha \rightleftharpoons \beta$ Transition in FeSi₂. *Phys. Status Solidi B* **51**(1), K85–K88 (1972)
165. W.A. Jensen et al., Eutectoid transformations in Fe–Si Alloys for thermoelectric applications. *J. Alloys Compd.* **721**, 705–711 (2017)
166. E. Weber, H.G. Rietz, The solution of iron in silicon. *J. Appl. Phys.* **51**(3), 1484–1488 (1980)
167. A.E. Rubin, C. Ma, Meteoritic minerals and their origins. *Chem. Erde Geochem.* **77**(3), 325–385 (2017)
168. Z. Yu, Two new minerals Gupeite and Xifengite in cosmic dusts from Yanshan. *Acta Petrol. Mineral. Anal.* **3**, 231–238 (1984)
169. K. Keil, J.L. Berkley, L.H. Fuchs, Suessite, Fe₃Si: a new mineral in the North Haig ureilite. *Am. Mineral.* **67**, 126–131 (1982)
170. M.I. Novgorodova et al., First occurrence of Suessite on the Earth. *Int. Geol. Rev.* **26**(1), 98–101 (1984)
171. M. Anand et al., New lunar mineral HAPKEITE*: product of impact-induced vapor-phase deposition in the regolith? in *Proc. Lunar and Planetary Science Conference XXXIV*, (2003), p. 1818
172. N. Shi et al., Naquite, FeSi, a new mineral species from Luobusha, Tibet, Western China. *Acta Geol. Sin. (Engl. Ed.)* **86**(3), 533–538 (2012)
173. G. Li et al., Linzhiite, FeSi₂, a redefined and revalidated new mineral species from Luobusha, Tibet, China. *Eur. J. Mineral.* **24**(6), 1047–1052 (2012)
174. R.A. Fischer et al., Phase relations in the Fe–FeSi system at high pressures and temperatures. *Earth Planet. Sci. Lett.* **373**, 54–64 (2013)
175. R.A. Fischer et al., Equation of state and phase diagram of Fe–16Si alloy as a candidate component of Earth’s core. *Earth Planet. Sci. Lett.* **357–358**, 268–276 (2012)
176. C.J. Allègre et al., The chemical composition of the Earth. *Earth Planet. Sci. Lett.* **134**(3), 515–526 (1995)
177. J. Wade, B.J. Wood, Core formation and the oxidation state of the Earth. *Earth Planet. Sci. Lett.* **236**(1), 78–95 (2005)
178. B. Martorell et al., The elastic properties of hcp-Fe_{1-x}Si_x at Earth’s inner-core conditions. *Earth Planet. Sci. Lett.* **451**, 89–96 (2016)
179. M.C.M. Farquhar, H. Lipson, A.R. Weill, An X-ray study of iron-rich iron-silicon alloys. *J. Iron Steel Inst.* **152**, 457–472 (1945)
180. F. Lihl, H. Ebel, Röntgenographische Untersuchungen über den Aufbau eisenreicher Eisen-Silizium-Legierungen. *Arch. Eisenhüttenwes.* **32**(7), 489–491 (1961)
181. F. Richter, W. Pepperhoff, The lattice constant of ordered and disordered iron-silicon alloys. *Arch. Eisenhüttenwes.* **45**, 107–109 (1974)
182. E.A. Kümmerle et al., Thermal formation of vacancies in Fe₃Si. *Phys. Rev. B* **52**(10), R6947–R6950 (1995)
183. A. Gude, H. Mehrer, Diffusion in the D0₃-type intermetallic phase Fe₃Si. *Philos. Mag. A* **76**(1), 1–29 (1997)
184. G.E. Lakso, M.J. Marcinkowski, Plastic deformation behavior in the Fe₃Si superlattice. *Trans. Metall. Soc. AIME* **245**, 1111–1120 (1969)
185. G.E. Lakso, M.J. Marcinkowski, Plastic deformation in Fe–Si alloys. *Metall. Trans.* **5**(4), 839–845 (1974)
186. S.K. Ehlers, M.G. Mendiratta, Tensile behaviour of two D0₃-ordered alloys: Fe₃Si and Fe-20 at % Al-5 at % Si. *J. Mater. Sci.* **19**(7), 2203–2210 (1984)
187. T.D. Yensen, The magnetic properties of some iron alloys melted in Vacuo. *Trans. Am. Inst. Electr. Eng.* **34**(2), 2601–2670 (1915)
188. M.G. Corson, The constitution of the Fe-silicon alloys, particularly in connection with the properties of corrosion-resisting alloys of this composition. *Trans. AIME* **80**, 249–296 (1928)

189. L.K. Varga et al., Structural and magnetic properties of metastable $\text{Fe}_{1-x}\text{Si}_x$ ($0.15 < x < 0.34$) alloys prepared by a rapid-quenching technique. *J. Phys. Condens. Matter.* **14**(8), 1985 (2002)
190. W.F. Barrett, W. Brown, R.A. Hadfield, On the electrical conductivity and magnetic permeability of various alloys of iron. *Sci. Trans. R. Dublin Soc.* **7**(Series 2), 67–126 (1900)
191. J.L. Haughton, M.L. Becker, Alloys of iron research. IX. The constitution of the alloys of iron with silicon. *J. Iron Steel Inst.* **121**, 315–335 (1930)
192. M. Fallot, Ferromagnetism of iron alloys (in French). *Ann. Phys. (Paris, Fr.)* **11**(6), 305–387 (1936)
193. M.K. Kolel-Veetil et al., Carbon nanocapsule-mediated formation of ferromagnetic Fe_5Si_3 nanoparticles. *J. Phys. Chem. C* **113**(33), 14663–14671 (2009)
194. L.K. Varga et al., Magnetic properties of rapidly quenched $\text{Fe}_{100-x}\text{Si}_x$ ($15 < x < 34$) alloys. *Mater. Sci. Eng. A* **304-306**, 946–949 (2001)
195. J.E. Wittig, G. Frommeyer, Deformation and fracture behavior of rapidly solidified and annealed iron-silicon alloys. *Metall. Mater. Trans. A* **39**, 252–265 (2008)
196. D. Hawezy, The influence of silicon content on physical properties of non-oriented silicon steel. *Mater. Sci. Technol.* **33**(14), 1560–1569 (2017)
197. H.H. Uhlig, R.W. Revie, *Corrosion and Corrosion Control – An Introduction to Corrosion Science and Engineering*, 3rd edn. (Wiley, New York, 1985), p. 458
198. S. Yamaguchi, An electron diffraction study of the protective coating on metals and alloys (continued): the acid-proof surface of ferrosilicon (Duriron). *Bull. Chem. Soc. Jpn.* **16**(9), 332–335 (1941)
199. R. Wasmuht, Über Konstitution und Eigenschaften des säurebeständigen Silicium-Eisengusses (About constitution and properties of acid-proof silicon-iron castings). *Angew. Chem.* **45**(36), 569–573 (1932)
200. R.K. Roy et al., Development of rapidly solidified 6.5 wt% silicon steel for magnetic applications. *Trans. Indian Inst. Met.* **63**(4), 745–750 (2010)
201. Y. Takada et al., Commercial scale production of Fe-6.5 wt. % Si sheet and its magnetic properties. *J. Appl. Phys.* **64**(10), 5367–5369 (1988)
202. F. Fiorillo, Advances in Fe-Si properties and their interpretation. *J. Magn. Magn. Mater.* **157-158**, 428–431 (1996)
203. K. Fujita, M. Namikawa, Y. Takada, Magnetic properties and workability of 6.5% Si steel sheet manufactured by siliconizing process. *J. Mater. Sci. Technol.* **16**(2), 137–140 (2000)
204. T. Ros-Yañez, Y. Houbaert, V. Gómez Rodríguez, High-silicon steel produced by hot dipping and diffusion annealing. *J. Appl. Phys.* **91**(10), 7857–7859 (2002)
205. C. Bolfarini et al., Magnetic properties of spray-formed Fe–6.5%Si and Fe–6.5%Si–1.0%Al after rolling and heat treatment. *J. Magn. Magn. Mater.* **320**(20), e653–e656 (2008)
206. J.H. Yu et al., The effect of heat treatments and Si contents on B2 ordering reaction in high-silicon steels. *Mater. Sci. Eng. A* **307**(1), 29–34 (2001)
207. R. Li et al., Magnetic properties of high silicon iron sheet fabricated by direct powder rolling. *J. Magn. Magn. Mater.* **281**(2), 135–139 (2004)
208. K. Arai, N. Tsuya, Ribbon-form silicon-iron alloy containing around 6.5 percent silicon. *IEEE Trans. Magn.* **16**(1), 126–129 (1980)
209. K.N. Kim et al., The effect of boron content on the processing for Fe–6.5wt% Si electrical steel sheets. *J. Magn. Magn. Mater.* **277**(3), 331–336 (2004)
210. T. Doi, H. Ninomiya, High silicon steel sheet realizing excellent high frequency reactor performance, in *Twenty-Seventh Annual IEEE Applied Power Electronics Conference and Exposition (APEC)*, (2012), pp. 1740–1746
211. K. Senda, M. Namikawa, Y. Hayakawa, Electrical steels for advanced automobiles – core materials for motors, generators, and high-frequency reactors. *JFE Techn. Rep. No.* **4**, 1–7 (2004)
212. P.-W. Jang, B.-H. Lee, G.-B. Choi, Variation of magnetic properties of Fe-Si compressed cores with Si content. *J. Korean Magn. Soc.* **20**(1), 13–17 (2010)
213. P. Jang, G. Choi, Acoustic noise characteristics and magnetostriction of Fe-Si powder cores. *IEEE Trans. Magn.* **48**(4), 1549–1552 (2012)

214. B. You et al., Optimization of powder core inductors of buck-boost converters for Hybrid Electric Vehicles, in *2009 IEEE Vehicle Power and Propulsion Conference*, (2009)
215. B. You et al., Experimental comparison of Mega Flux and JNEX inductors in high power dc-dc converter of Hybrid Electric Vehicles, in *2011 IEEE Vehicle Power and Propulsion Conference*, (2011)
216. M.S. Rylko, J.G. Hayes, M.G. Egan, Experimental investigation of high-flux density magnetic materials for high-current inductors in hybrid-electric vehicle DC-DC converters, in *2010 IEEE Vehicle Power and Propulsion Conference*, (2010)
217. K. Lee et al., A study on the performance of 10kW Grid-Connected Photovoltaic power conditioning system with characteristics variation in inductor core materials, in *The 2010 International Power Electronics Conference – ECCE ASIA*, (2010)
218. H. Masumoto, T. Yamamoto, On a new alloy “Sendust” and its magnetic and electric properties. *J. Jpn. Inst. Met.* **1**(3), 127–135 (1937)
219. H.H. Helms Jr., E. Adams, Sendust sheet-processing techniques and magnetic properties. *J. Appl. Phys.* **35**(3), 871–872 (1964)
220. N. Tsuya et al., Magnetic recording head using ribbon-sendust. *IEEE Trans. Magn.* **17**(6), 3111–3113 (1981)
221. T. Kobayashi et al., A tilted sendust sputtered ferrite video head. *IEEE Trans. Magn.* **21**(5), 1536–1538 (1985)
222. S. Yoshida et al., Permeability and electromagnetic-interference characteristics of Fe–Si–Al alloy flakes–polymer composite. *J. Appl. Phys.* **85**(8), 4636–4638 (1999)
223. K. Nomura et al., Mössbauer study on Fe-Si-Al flakes-polymer composites for noise filter at high frequency bands. *J. Jpn. Soc. Powder Powder Metall.* **50**(4), 260–265 (2003)
224. P. Winkler, W. Günther, Enlarging the standard permeability set of powder e-cores by combination of different perm core-halves, in *PCIM Europe 2018; International Exhibition and Conference for Power Electronics, Intelligent Motion, Renewable Energy and Energy Management*, (2018)
225. K. Yoo, B.K. Lee, D. Kim, Investigation of vibration and acoustic noise emission of powder core inductors. *IEEE Trans. Power Electron.*, 1–1 (2018)
226. M.G. Mendiratta, H.A. Lipsitt, D0₃-domain structures in Fe₃Al-X alloys. *Mat. Res. Soc. Symp. Proc.* **39**, 155–162 (1985)
227. B.K. Grant, *International directory of company histories*, vol 17 (St. James Press, Detroit, 1997), p. 736
228. P.D. Schenck, Acid resisting irons. *Chem. Metall. Eng.* **28**, 678 (1923)
229. O. Schneeweiss et al., Fe₃Si surface coating on SiFe steel. *J. Magn. Magn. Mater.* **215–216**, 115–117 (2000)
230. A. Ionescu et al., Structural, magnetic, electronic, and spin transport properties of epitaxial Fe₃Si/GaAs(001). *Phys. Rev. B* **71**(9), 094401 (2005)
231. J. Herfort et al., Epitaxial growth of Fe₃Si/GaAs(001) hybrid structures for spintronic application. *J. Cryst. Growth* **278**(1), 666–670 (2005)
232. R. Mantovan et al., Synthesis and characterization of Fe₃Si/SiO₂ structures for spintronics. *Phys. Status Solidi A* **205**(8), 1753–1757 (2008)
233. R. Nakane, M. Tanaka, S. Sugahara, Preparation and characterization of ferromagnetic D0₃-phase Fe₃Si thin films on silicon-on-insulator substrates for Si-based spin-electronic device applications. *Appl. Phys. Lett.* **89**(19), 192503 (2006)
234. N. Dahal, V. Chikan, Phase-Controlled Synthesis of Iron Silicide (Fe₃Si and FeSi₂) Nanoparticles in Solution. *Chem. Mater.* **22**(9), 2892–2897 (2010)
235. M. Rudy, I. Jung, G. Sauthoff, Ferritic Fe-Al-Ni alloys for high temperature applications, in *High Temperature Alloys – Their Exploitable Potential*, (Elsevier, London/New York, 1987)
236. C.T. Sims, A history of superalloy metallurgy for superalloy metallurgists, in *Superalloys 1984*, (TMS-AIME, Warrendale, 1984)
237. A. Kracke, Superalloys, the most successful alloy system of modern times – past, present and future, in *7th International Symposium on Superalloy 718 and its Derivatives*, (TMS, Warrendale, 2010)

238. V. Seetharaman, M. Sundararaman, R. Krishnan, Precipitation hardening in a PH 13-8 Mo stainless steel. *Mater. Sci. Eng.* **47**, 1–11 (1981)
239. W.M. Garrison, R. Strychor, A preliminary study of the influence of separate and combined aluminum and nickel additions on the properties of a secondary hardening steel. *Metal. Trans.* **19A**(12), 3103–3107 (1988)
240. R. Hamano, The effect of the precipitation of coherent and incoherent precipitates on the ductility and toughness of high-strength steel. *Metall. Trans.* **24A**(1), 127–139 (1993)
241. S. Jiang et al., Ultrastrong steel via minimal lattice misfit and high-density nanoprecipitation. *Nature* **544**, 460–465 (2017)
242. Y. Liao, I. Baker, Microstructure and room-temperature mechanical properties of Fe₃₀Ni₂₀Mn₃₅Al₁₅. *Mater. Charact.* **59**, 1546–1549 (2008)
243. I. Jung, G. Sauthoff, Creep behaviour of the intermetallic B2 phase (Ni,Fe)Al with strengthening soft precipitates. *Z. Metallkd.* **80**(7), 484–489 (1989)
244. M.J.S. Rawlings et al., Effect of titanium additions upon microstructure and properties of precipitation-strengthened Fe-Ni-Al-Cr ferritic alloys. *Acta Mater.* **128**, 103–112 (2017)
245. S.I. Baik et al., Increasing the creep resistance of Fe-Ni-Al-Cr superalloys via Ti additions by optimizing the B2/L2₁ ratio in composite nano-precipitates. *Acta Mater.* **157**, 142–154 (2018)
246. H.A. Calderon, M.E. Fine, J.R. Weertman, Coarsening and morphology of β' particles in Fe-Ni-Al-Mo ferritic alloys. *Metall. Trans. A* **19**(5), 1135–1146 (1988)
247. G. Song et al., Ferritic alloys with extreme creep resistance via coherent hierarchical precipitates. *Sci. Rep.* **5**, 16327 (2015)
248. S.I. Baik, M. Rawlings, D.C. Dunand, Effect of hafnium micro-addition on precipitate microstructure and creep properties of a Fe-Ni-Al-Cr-Ti ferritic superalloy. *Acta Mater.* **153**, 126–135 (2018)
249. S.M. Zhu, S.C. Tjong, J.K.L. Lai, Creep behavior of a β'(NiAl) precipitation strengthened ferritic Fe-Cr-Ni-Al alloy. *Acta Mater.* **46**(9), 2969–2976 (1998)
250. Y. Zhao et al., Creep behavior as dislocation climb over NiAl nanoprecipitates in ferritic alloy: the effects of interface stresses and temperature. *Int. J. Plast.* **69**, 89–101 (2015)
251. C. Stallybrass, A. Schneider, G. Sauthoff, The strengthening effect of (Ni,Fe)Al precipitates on the mechanical properties at high temperatures of ferritic Fe-Al-Ni-Cr alloys. *Intermetallics* **13**(12), 1263–1268 (2005)
252. Z.K. Teng et al., Room temperature ductility of NiAl-strengthened ferritic steels: effects of precipitate microstructure. *Mater. Sci. Eng. A* **541**, 22–27 (2012)
253. Z.Q. Sun et al., Duplex precipitates and their effects on the room-temperature fracture behaviour of a NiAl-strengthened ferritic alloy. *Mater. Res. Lett.* **3**(3), 128–134 (2015)
254. M.D. Bhandarkar et al., Structure and elevated temperature properties of carbon-free ferritic alloys strengthened by a Laves phase. *Metall. Trans. A* **6**(6), 1281–1289 (1975)
255. S. Muneki et al., Creep characteristics in carbon free new martensitic alloys. *Mater. Sci. Eng. A* **406**, 43–49 (2005)
256. F. Wever, W. Peter, Ausscheidungshärtung und Dauerstandfestigkeit von Eisen-Niob-Legierungen und nioblegierten Stählen. *Arch. Eisenhuettenwes.* **15**(8), 357–363 (1942)
257. J.S. Lee et al., Causes of breakdown of creep strength in 9Cr–1.8W–0.5Mo–VNb steel. *Mater. Sci. Eng. A* **428**(1–2), 270–275 (2006)
258. F. Abe, Effect of fine precipitation and subsequent coarsening of Fe₂W Laves phase on the creep deformation behavior of tempered martensitic 9Cr-W steels. *Metall. Mater. Trans. A* **36**(2), 321–332 (2005)
259. M.G. Gemmill et al., Study of 7% and 8% chromium creep-resistant steels. *J. Iron Steel Inst.* **184**(10), 122–144 (1956)
260. V. Foldyna et al., Evaluation of structural stability and creep resistance of 9–12% Cr steels. *Steel Res.* **67**(9), 375–381 (1996)
261. J. Hald, Metallurgy and creep properties of new 9–12%Cr steels. *Steel Res.* **67**(9), 369–374 (1996)

262. O. Prat et al., The role of Laves phase on microstructure evolution and creep strength of novel 9%Cr heat resistant steels. *Intermetallics* **32**, 362–372 (2013)
263. B. Kuhn et al., Development of high chromium ferritic steels strengthened by intermetallic phases. *Mater. Sci. Eng. A* **594**, 372–380 (2014)
264. N. Kanno et al., Mechanical properties of austenitic heat-resistant Fe–20Cr–30Ni–2Nb steel at ambient temperature. *Mater. Sci. Eng. A* **662**, 551–563 (2016)
265. M. Shibuya et al., Effect of nickel and cobalt addition on the precipitation-strength of 15Cr ferritic steels. *Mater. Sci. Eng. A* **528**, 5387–5393 (2011)
266. J. Froitzheim et al., Development of high strength ferritic steel for interconnect application in SOFCs. *J. Power Sources* **178**, 163–173 (2008)
267. L. Niewolak et al., Temperature dependence of phase composition in W and Si-alloyed high chromium ferritic steels for SOFC interconnect applications. *J. Alloys Compd.* **717**, 240–253 (2017)
268. B. Kuhn et al., Effect of Laves phase strengthening on the mechanical properties of high Cr ferritic steels for solid oxide fuel cell interconnect application. *Mater. Sci. Eng. A* **528**, 5888–5899 (2011)
269. B. Kuhn et al., Development status of higher performance ferritic (HiperFer) steels, in *8th International Conference on Advances in Materials Technology for Fossil Power Plants (EPRI 2016)*, (ASM International, Materials Park, 2016)
270. I. Tarigan et al., Novel concept for creep strengthening mechanism using grain boundary Fe₂Nb Laves phase in austenitic heat resistant steel. *Mater. Res. Soc. Symp. Proc.* **1295**, 317–322 (2011)
271. M. Takeyama, Novel concept of austenitic heat resistant steels strengthened by intermetallics. *Mater. Sci. Forum* **539–543**, 3012–3017 (2007)
272. Lyta et al., Microstructure development of oxide scale during steam oxidation of the Fe₂₀Cr₃₀Ni₂Nb (at%) austenitic steel at 1073K. *Mater. Trans. JIM* **54**(12), 2276–2284 (2013)